LASER INTERFEROMETER GRAVITATIONAL WAVE OBSERVATORY

- LIGO -

LIGO Laboratory / LIGO Scientific Collaboration

Document Type	**LIGO-T1100071**	Oct/18/2011

Frequency Domain Calibration Error Budget for LIGO in S6

I. Bartos, I. Belopolski, J. Berliner, J. Burguet-Castell, R. De Rosa, P. Daveloza, A. Effler, T. Fricke, G. Gonzalez, K. Kawabe, M. Landry, G. Meadors, G. Mendell, J. Rollins, R. Savage, X. Siemens, M. Sung, D. Yeaton-Massey

This is an internal working note
of the LIGO Project.

California Institute of Technology
LIGO Project - MS 18-34
1200 E. California Blvd.
Pasadena, CA 91125
Phone (626) 395-2129
Fax (626) 304-9834
E-mail: info@ligo.caltech.edu

Massachusetts Institute of Technology
LIGO Project - NW17-161
175 Albany St.
Cambridge, MA 01239
Phone (617) 253-4824
Fax (617) 253-7014
E-mail: info@ligo.mit.edu

LIGO Hanford Observatory
P.O.Box 1970
Mail Stop S9-02
Richland WA 99352
Phone (509) 372-8106
Fax (509) 372-8137

LIGO Livingston Observatory
P.O.Box 940
Livingston, LA 70754
Livingston LA 70754
Phone (225) 686-3100
Fax (225) 686-7189

http//www.ligo.caltech.edu/

Contents

Abstract

S6 error budget of the version 2 (V2) frequency domain calibration is explained. The analysis method is substantially different from S5 due to the introduction of so-called open loop residual in the model.

1 Summary

Caution: This document is still a work in progress. As of version 5 of this document, this summary shows the calibration error estimate for the entire S6, and all of the numbers in this summary as well as the method used for the analysis have been vetted. However, readers should be careful as many sections of this document are still written as if they only target the blind injection.

LIGO data generation goes through two stages. First a frequency domain model colloquially called $h(f)$ is constructed as a set of transfer functions and scaling factors, and then this model is transfered to the time domain model colloquially called $h(t)$ which is used for the production of the LIGO strain data stream.

We categorize errors in the frequency domain response function R into four: Overall scaling error that is independent of frequency, frequency dependent error except timing error, timing error, and time evolution error that is related to the random error in so-called calibration factor. This is written by

$$
\begin{aligned}
R(f) &= \eta_R(f) R_M(f) \\
&= A_0 \left(1 + \delta A_+ - \delta A_-\right) \eta_R^0(f) \exp\left(-2i\pi f \tau_R\right) \eta_\gamma(f) R_M(f) \\
&= A_0 \left(1 + \delta A_+ - \delta A_-\right) \mathrm{abs}\left(\eta_R^0(f)\right) \exp\left[i(\Delta\phi_R(f) - 2\pi f \tau_R)\right] \eta_\gamma(f) R_M(f) \quad (1.1)
\end{aligned}
$$

where R and R_M are "true" and V2 model response function, η_R is the ratio of the two, A_0 and $\delta A_\pm$ are the overall scaling error that is equal to the scaling factor of the actuation, η_R^0 is the frequency-dependent part of η_R except the timing error and the time evolution error,

$\Delta\phi_R$ is the phase of η_R^0, τ_R is the timeing error, and η_γ is the time evolution error. Note that we define "timing error" as any phase systematic that is proportional to the frequency within LIGO calibration band of [40, 5000] Hz.

The time domain data has all of the errors present in the frequency domain data, but there might be an additional error related to the conversion from the frequency domain model to the time domain. We performed two independent tests to make a comparison between $h(f)$ and $h(t)$ [1] to obtain a conventional error estimate.

Figure 1.1 and 1.2 show the overall scaling, the frequency dependence, and the time evolution error for L1 and H1 frequency domain response function. Table 1 shows the recommendation for a conventional error for $h(t)/h(f)$ difference. Though the analysis groups can use the figures and the table to suite their needs, Table 2 summarizes the recommendation of the Calibration Committee.

There are several things one needs to know to correctly use and understand the LIGO calibration.

IFO	Epoch	[40, 2000] Hz	[2000, 5000] Hz
L1	S6a	3 %, 4 degrees	3.5 %, 12 degrees
	S6b	7 %, 3.5 degrees	4 %, 2 degrees
H1	S6a	4 %, 2 degrees	6 %, 4.5 degrees
	S6b	3 %, 2 degrees	6.5 %, 5 degrees

Table 1: Recommendation for a conventional estimate of $h(f)/h(t)$ difference error obtained from two independent tests.

1.1 Calibration Epoch

In V2 calibration, there are two calibration epochs often called S6a and S6b (Tab.3). This comes from a large enough change in the interferometer configuration at both of the sites. Note that, despite similar naming, these are not to be confused with the epochs used by the analysis groups.

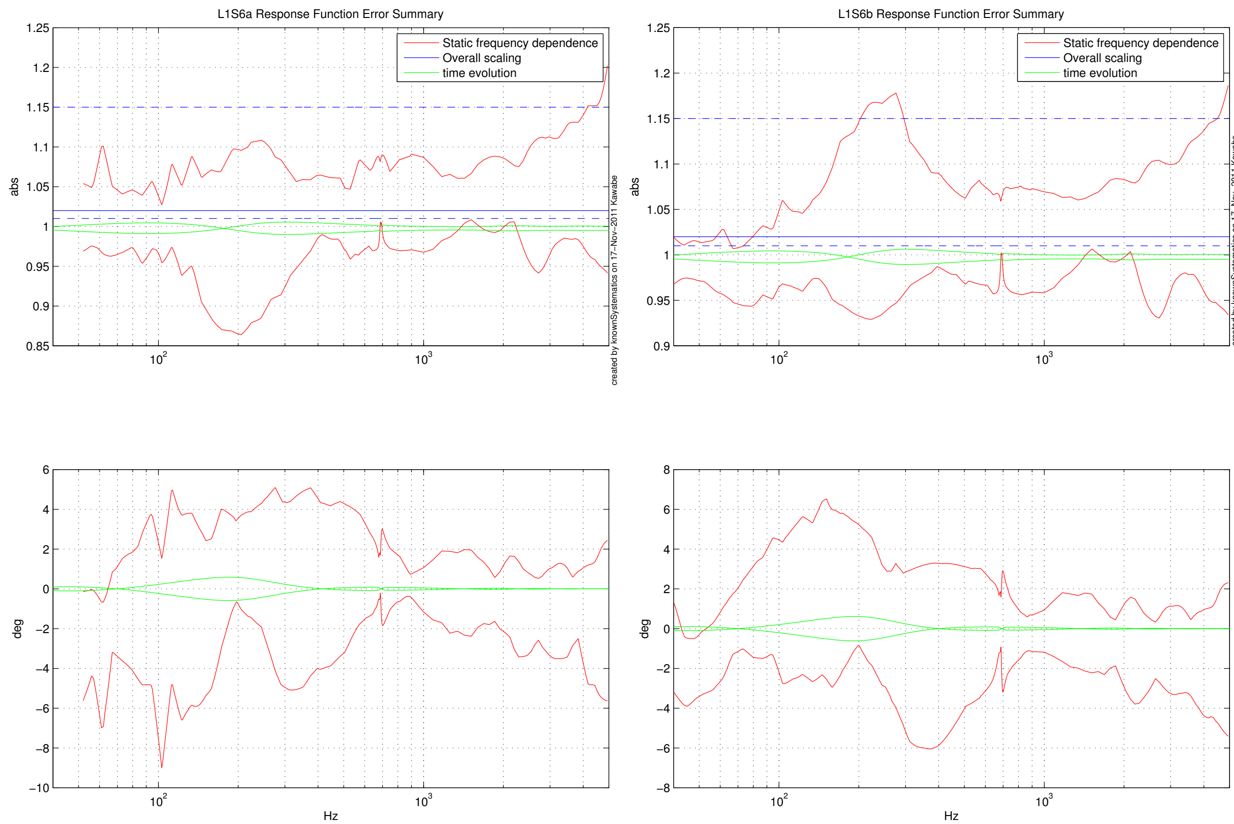

Figure 1.1: Summary of L1 frequency domain response function error (except the timing error) for the S6a and S6b calibration epoch. The time evolution error is much smaller than the static frequency dependence error and thus can be neglected. For time domain calibration (colloquially called $h(t)$ calibration), we recommend to add a conservative error in Table 1 in quadrature to the frequency dependent error. Note that the error range of the frequency dependent error is dominated by the fact that multiple hardware/software configurations and states are covered by one calibration model per epoch.

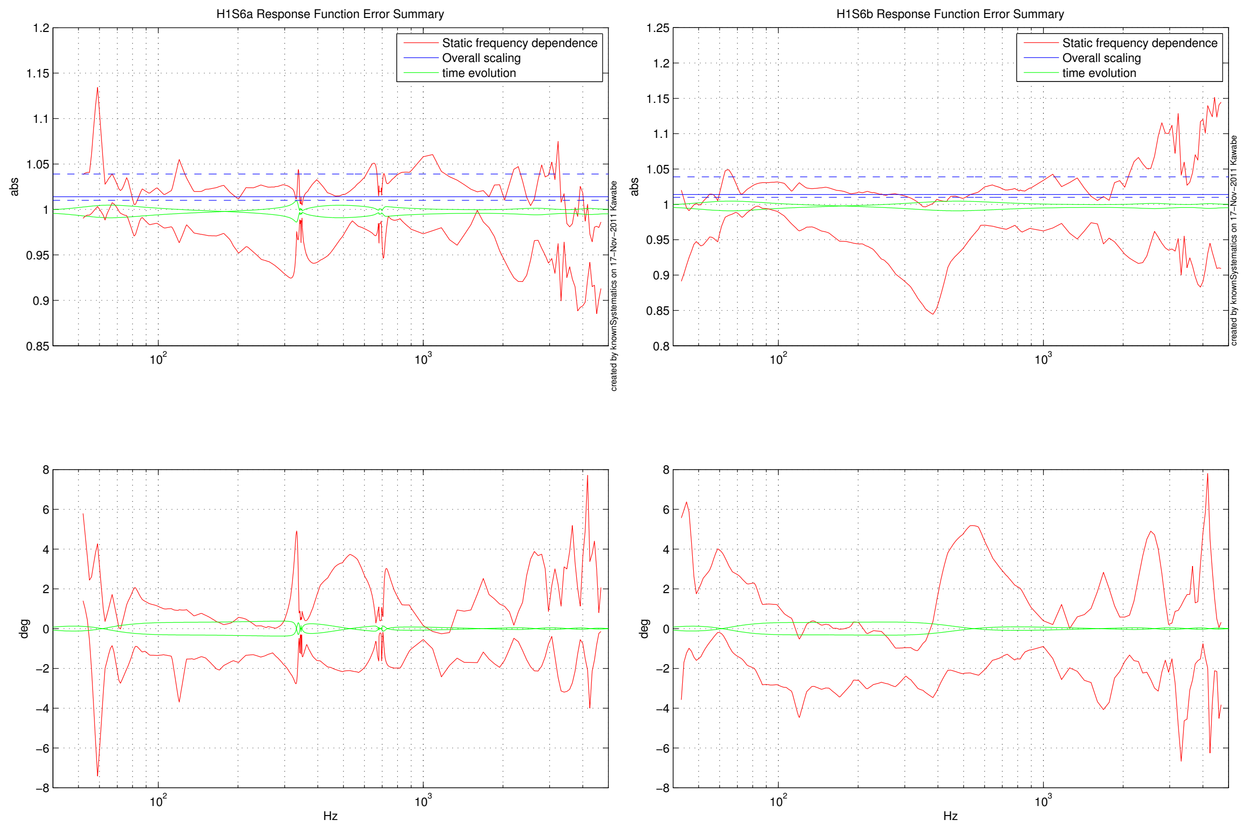

Figure 1.2: Summary of H1 frequency domain response function error (except the timing error) for the S6a and S6b calibration epoch. For time domain calibration, we recommend to add a conservative error in Table 1 in quadrature to the frequency dependent error. Because of the actuation anomaly in H1 EY, any analysis using [3000,4000]Hz band should inflate the error for that band to 40% in amplitude and 27 degrees in phase. Note that the error range of the frequency dependent error is dominated by the fact that multiple hardware/software configurations and states are covered by one calibration model per epoch.

L1	Overall scaling $= 1.02(1+0.13\text{-}0.01)$ Timing error $= [-10, +45]\mu$s				
	Static frequency dependence recommendation				
	Epoch		[40, 70] Hz	[70, 2000] Hz	[2000, 5000] Hz
	S6a	$\lvert h(f)\rvert$	10%	14 %	20%
		$\lvert h(t)\rvert$	$\sqrt{10^2+3^2} = 10$ %	$\sqrt{14^2+3^2} = 14$ %	$\sqrt{20^2+3.5^2} = 20$%
		$\angle h(f)$	7 deg	9 deg	6 deg
		$\angle h(t)$	$\sqrt{7^2+4^2} = 8$ deg	$\sqrt{9^2+4^2} = 10$ deg	$\sqrt{6^2+12^2} = 13$ deg
	S6b	$\lvert h(f)\rvert$	5%	18%	19%
		$\lvert h(t)\rvert$	$\sqrt{5^2+7^2} = 9$ %	$\sqrt{18^2+7^2} = 19$ %	$\sqrt{19^2+4^2} = 19$ %
		$\angle h(f)$	4 deg	7 deg	5 deg
		$\angle h(t)$	$\sqrt{4^2+3.5^2} = 5$ deg	$\sqrt{7^2+3.5^2} = 8$ deg	$\sqrt{5^2+2^2} = 5$ deg
H1	Overall scaling $= 1.014(1+0.025\text{-}0.004)$ Timing error $= [0, +30]\mu$s				
	Static frequency dependence recommendation				
	Epoch		[40, 70] Hz	[70, 2000] Hz	[2000, 5000] Hz
	S6a	$\lvert h(f)\rvert$	13 %	8 %	40 %
		$\lvert h(t)\rvert$	$\sqrt{13^2+4^2} = 14$ %	$\sqrt{8^2+4^2} = 9$ %	$\sqrt{40^2+6^2} = 40$ %
		$\angle h(f)$	7 deg	5 deg	27 deg
		$\angle h(t)$	$\sqrt{7^2+2^2} = 7$ deg	$\sqrt{5^2+2^2} = 5$ deg	$\sqrt{27^2+4.5^2} = 27$ deg
	S6b	$\lvert h(f)\rvert$	11 %	16 %	40 %
		$\lvert h(t)\rvert$	$\sqrt{11^2+3^2} = 11$ %	$\sqrt{16^2+3^2} = 16$ %	$\sqrt{40^2+6.5^2} = 41$ %
		$\angle h(f)$	6 deg	5 deg	27 deg
		$\angle h(t)$	$\sqrt{6^2+2^2} = 6$ deg	$\sqrt{5^2+2^2} = 5$ deg	$\sqrt{27^2+5^2} = 28$ deg

Table 2: Recommendation for the error for the entire S6. The error for [2000,5000] Hz band for H1 was inflated using a very conservative assumptions because of our incomplete knowledge of EY actuation resonances in [3000,4000] Hz band. If [3000,4000] Hz band is excluded, you can use $\sqrt{11^2+6^2} = 13$ %, $\sqrt{8^2+4.5^2} = 9$ degrees for S6a, and $\sqrt{15^2+6.5^2} = 16$ %, $\sqrt{8^2+5^2} = 9$ degrees for S6b. A positive time delay means that the $h(f)$ signal or $h(t)$ signal is delayed from the physical strain (e.g. induced by gravitational wave).

	S6a	S6b
L1	[928368015, 938995214]	[941997600, end]
H1	[929904671, 942436810]	[942436815, end]

Table 3: Two calibration epochs in S6. Though these are often called S6a and S6b by the calibration group, these are not to be confused with the epochs used by the analysis groups.

1.2 Overall scaling factor

The overall scaling factor error is plotted as three lines ($A_0 \times [1, 1 + \delta A_+, 1 - \delta A_-]$). This didn't change for the entire S6 run. It directly comes from the error in the scaling factor of the coil-magnet actuator strength, and we do not expect this to change.

1.3 Frequency dependence covers multiple configurations and hardware states

The frequency dependent error changed through the run as interferometer hardware/software configurations (such as whitening/dewhitening mismatch for the OMC photo detectors) and hardware states (such as the ADC timing) changed. The calibration committee tracked these changes over the entire run and estimated the error for each and every configuration and hardware state. The frequency dependent error presented as a band in Figures 1.1 and 1.2 shows the maximum and minimum error, e.g. $[min(\eta_R^0), max(\eta_R^0)]$ for amplitude, per the calibration epoch. This is not a true representative of the statistical errors, as it includes relatively large known systematics of several configurations and many hardware states in addition to statistical errors associated with the measurements of relevant configurations and states. The calibration review committee concluded that it is safe to handle them as one-sigma error bar in that doing so would over estimate the error.

This means that, for any given time, the frequency dependent calibration error is understood with much better accuracy than Figures 1.1 and 1.2. If there arises a significant need to have a finer-grained calibration error analysis at a specific time, e.g. a potential detection candidate, the calibration committee can provide a much better estimate of the calibration. An example would be the calibration analysis for the blind hardware injection in S6b calibration period (see 9.4).

This also means that, by merely targeting a specific hardware/software configuration, even though it still includes many hardware states, you may find the calibration error that is more accurate than Figures 1.1 and 1.2 and Table 2. For example, for the most part of S6b except the gps time [948444884, 948539900] and [961827382, 961835000], H1 frequency domain error for [70, 2000]Hz range was 11% in amplitude and 3 degrees in phase rather than 15% and 5 degrees. See Figures 4.17, 4.18 and Table 10 for details.

1.4 Data flags

Several calibration-related data flags were made, i.e. one related to so-called spike glitches in L1, one related to abnormally large time offset, and one related to incorrect software configuration. The flagged data might still not be corrupt, however no serious attempt was made to validate the calibration for these data segments. The calibration committee can offer the community some general advice, however ultimately the analysts should decide how to handle the flagged segments.

1.5 High frequency for H1

Due to a resonant structure only in the H1 EY actuation (4.1.5), anybody planning to use [3000, 4000] Hz band should use a larger error of 40% in amplitude and 27 degrees in phase. This doesn't mean that the error is believed to this much. Rather, this is a conservative estimate of the calibration error which safely covers this frequency band even if our measurement doesn't capture the exact peaks and valleys of the resonant structure observed in EY. Figure 1.2 doesn't include this effect, but the Table 2 does. See 6 for details.

1.6 How to combine frequency dependence and overall scaling

If nessesary, the error bar of the overall scaling factor and the amplitude error of the frequency dependent part can be added in quadrature in Table 2 to make a combined amplitude error,

L1	S6a	$\sqrt{13^2+14^2} = 19$ %
	S6b	$\sqrt{13^2+19^2} = 23$ %
H1	S6a	$\sqrt{2.5^2+9^2} = 9.3$ %
	S6b	$\sqrt{2.5^2+16^2} = 16$ %

Table 4: Example of resulting amplitude error bar for [70, 2000] Hz. The relevant data are $|h(t)|$ and the scaling from Table 2. In addition to this error, the $h(t)$ scaling factor 1.02 (for L1) or 1.014 (for H1) has to be taken care of separately by either rescaling $h(t)$ or by changing the effective distance of the injections.

e.g. for L1 [70, 2000] Hz band for S6b, the overall amplitude error could be expressed as $1.02(1+\sqrt{0.13^2+0.19^2}-\sqrt{0.01^2+0.19^2}) = 1.02(1+0.23-0.19)$. Again the review concluded that it would be safe to use it as if it is a one sigma error bar even though the frequency dependent error band is not a true statistical error bar.

For example, one way to apply a *single* amplitude error bar for a search that uses only the [70, 2000] Hz band, taking the maximum of the scaling factor error and using Table 2, would be to use the values of Table 4.

Note that the overall scaling factor, 1.02 for L1 and 1.014 for H1, has to be taken into account by either rescaling the original $h(t)$ data itself or by correcting for the distance of the injections used in the analysis, effectively making them a factor of 1.02 or 1.014 *closer*.

2 Introduction

In LIGO calibration model, a LIGO instrument is represented by four elements colloquially called the sensing (C), the digital (D) and the actuation (A) functions, and the calibration factor (γ). Response function R is a function of these four:

$$R = \frac{1+\gamma CDA}{\gamma C} \equiv \frac{1+\gamma G}{\gamma C} \tag{2.1}$$

where G is the open loop transfer function of the control loop.

It's not within the scope of this document to explain what the above equation means.

This document does provide a detailed description of the error budget of R for the

	"True"	S6 Model	"True"/Model ratio	Fractional error
Response function	R	R_M	$\eta_R = R/R_M$	$\delta\eta_R = \eta_R - 1$
Sensing	C	C_M	$\eta_C = C/C_M$	$\delta\eta_C = \eta_C - 1$
Actuation	A	$A_M = A_{M0} \times Res_M e^{-2\pi i f \tau_M}$	$\eta_A = A/A_M$	$\delta\eta_A = \eta_A - 1$
Digital	D	$D_M = D$	1	0
OLG	G	$G_M = A_M C_M D_M$	$\eta_G = \eta_C\eta_A = G/G_M$	$\delta\eta_G = \eta_G - 1$
Calibration factor	$\gamma(t)$	$\gamma_M(t)$	$\eta_\gamma(t) = \gamma(t)/\gamma_M(t)$	

Table 5: Naming convention. A_{M0} is the actuation model constructed from known elements. So-called "OLG residual" represented by Res_M is put in the actuation model to take care of the bulk of discrepancy between the OLG model and the OLG measurements at high kHz. Likewise, an ad-hoc time delay parameter τ_M is put in the actuation to take care of the latency discrepancy between the OLG model and the OLG measurements.

frequency domain calibration. We will explore uncertainties and known systematics in each part of the model and study how these propagate to the uncertainties and systematic error in R.

2.1 Naming Convention

Elements in the V2 calibration model have subscript "M".

The ratio of the "true" physical quantity and the model is represented by η, e.g. $\eta_A = A/A_M$.

Fractional errors are prepended by δ, i.e. a fractional error associated with η is $\delta\eta = \eta - 1$.

Models are constructed only from components known at the time of constructing the model, except two systematic of unknown origin called open loop gain residual (OLG residual) and a small ad-hoc time delay parameter (see 4.1.7 for details).

Note that there are systematics that are not in the model but identified with very good accuracy after publishing the model, which are explained in 2.2.

A symbol θ is used for systematics of known quantity that are not explicitly put in the model. Whenever it is appropriate, a phase systematic that can be regarded as a true timing

	Symbol	Origin	Affects
Actuation coefficient error	A_0, $\delta A_\pm$	A	overall scaling
White/dewhite mismatch	θ_{wh}	C	frequency dependence
Arm poles error	θ_{arm}	C	frequency dependence
EY abnormal resonance	θ_Y	A	frequency dependence
Normal mass deformation	θ_{mass}	A	frequency dependence
ADC time delay	τ_{ADC}	C	frequency dependence
Latency between sensing CPUs	τ_{CPU}	C	frequency dependence
Control loop latency mismatch	τ_G	A and C	frequency dependence
Calibration factor error	θ_γ	C	time evolution error
OLG mismatch	θ_{OLG} $= \eta_G \exp(-2i\pi f \tau_G)$	Unknown	frequency dependence
OLG residual	Res_M	Unknown, put in A	frequency dependence
Ad-hoc delay	τ_M	Unknown, put in A	frequency dependence

Table 6: Table of the elements in the calibration error budget. The latency between the two sensing CPUs is in the model, and we consider only the deviation from the model here. OLG residual and ad-hoc delay are two elements that were explicitly put in the model as a buffer to fold into calibration the combined effect of all known and unknown errors that are not explicitly in the model.

error is represented by a symbol τ separately from a systematic that is not proportional to the frequency which is represented by $\Delta\phi$.

2.2 Error Elements in LIGO Instruments

Elements that are known to the calibration group to potentially affect the calibration of LIGO instruments were measured and analyzed. Out of these, twelve systematics listed in Table 6 were explicitly put in the error budget. These are explained in detail in the following sections.

For the systematics that are not explicitly in the error budget (but nevertheless measured and evaluated), see Sec.8 and Tab.9.

3 Overall Scaling Coefficient Error

In S6, the strength of the coil-magnet actuators were measured by two techniques. One uses the Michelson interferometer (MICH) to calibrate the ITM actuation and transfer it to

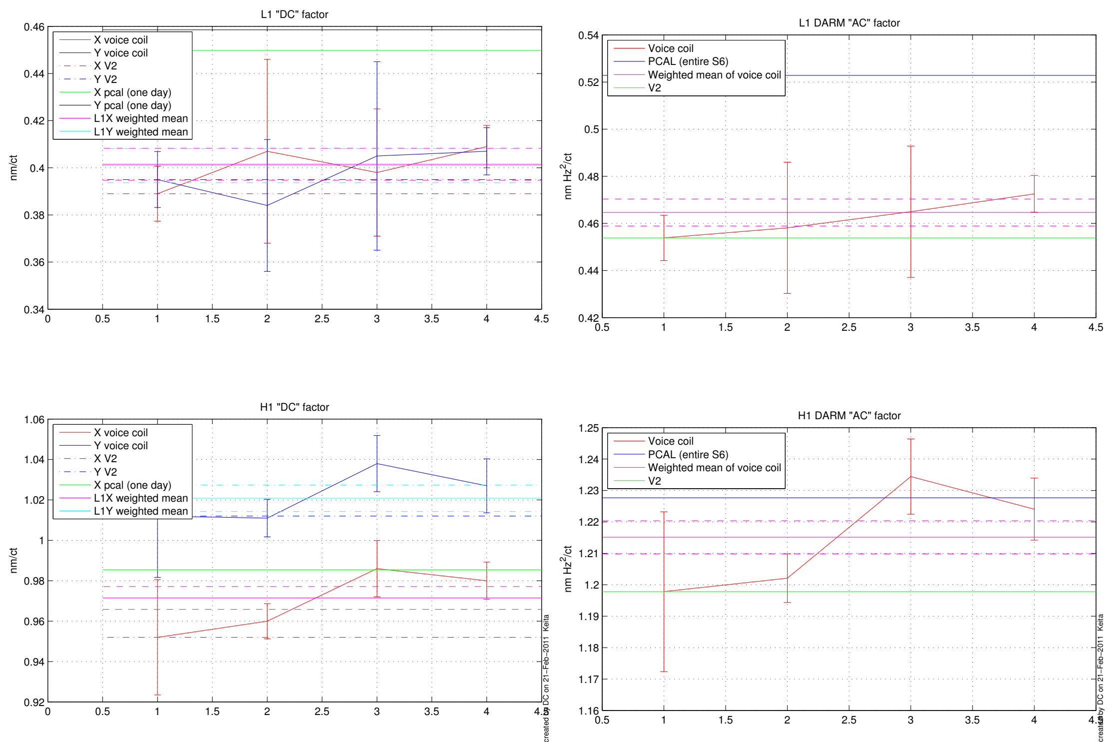

Figure 3.1: Actuation coefficient for each of the masses (left) and the combined DARM actuation coefficient (right).

the ETMs, and the other pushes the ETMX using radiation pressure of an auxiliary laser colloquially called photon calibrator or Pcal.

Figure 3.1 and Table 7 show the result of the analysis of the scaling coefficient. Note that V2 model was generated by one set of MICH measurement, but there are three more MICH data set with smaller error bars. MICH numbers in the table is a combined number of four sets, and the error bar is the standard error combining four standard deviation taken from four data set. For a full description of measurements, see the calibration review wiki[2].

As one can see, Pcal and latest MICH results agree within one per cent for H1. There used to be larger discrepancy, which was resolved by a careful measurement of the transmissivity of the viewport window for Pcal injection after EX vacuum chamber was opened. V2 number and latest MICH number differs by about 1 %, and the end result is about a factor of 1.014 mean plus 2.5% minus 0.4% error bar.

This is not the case with L1. There is about 13% difference between Pcal and the latest

	V2 [nm Hz^2/ct]	MICH [nm Hz^2/ct]	Pcal [nm Hz^2/ct]	$A_0(1+\delta A_+ - \delta A_-)$
L1	0.454	0.464(1±0.012)	0.523	1.02(1+0.13-0.01)
H1	1.198	1.215(1±0.004)	1.228	1.014(1+0.025-0.004)

Table 7: DARM Actuation Scaling Coefficient for S6.

MICH numbers VS about 2% between V2 and the latest MICH, and as a result we decided to take a factor of 1.02 plus 13% minus 1% error bar. The error is dominated by the systematic difference between MICH and Pcal. Note that the transmissivity of Pcal viewport was not remeasured for L1, as the vacuum chamber is still closed.

Though the actuation function does not explicitly appear in Eq.2.1, the actuation scaling error is equal to the response scaling error as suggested by Eq.1.1. This is because of the way the LIGO instruments are measured and modeled. Of the three components (C, A and D), the sensing function is something we cannot directly measure. We use another measurable quantity G as a boundary condition such that the overall scale of C is defined by $G/(AD)$. Any overall scaling error in A is equal to the inverse of the scaling error in C. Since the response function is inversely proportional to C, the overall scaling error in R is equal to the overall scaling error in A.

4 Frequency Dependent Error

We'll first look at each independent element contributing to the error, then combine them together to get a frequency dependent error in the closed loop response $1 + G$, the sensing C, and finally the response function R.

Since some of the elements are specific to the interferometer configuration, the ADC timing and the latency in DARM loop, the latter two being dependent on CPU initialization etc., the most detailed error budget should be generated for each of the distinctive configurations, ADC timing and a latency mismatch observed.

In this document, however, such a detailed analysis was only done to one period from September 14 2010 to the end of S6. For any other periods, we make one error budget per calibration epoch that covers all configurations and hardware status that are applicable.

4.1 Error Components

4.1.1 Whitening/dewhitening mismatch

The matching of analog whitening filter and digital dewhitening filter for OMC ADC is not perfect, and this is not accounted for in the V2 model. We call this systematic θ_{wh}.

For L1, people used four different configurations for OMC whitening filters: FM1/FM2 for both PD1 and PD2 (θ_{wh}^{0}), FM1/FM2/FM3 for both PD1 and PD2 (θ_{wh}^{FM123}), FM1/FM2/FM3 for PD1 and FM1 for PD2 (θ_{wh}^{test1}), and FM1/FM2 for PD1 and FM1/FM2/FM3 for PD2 (θ_{wh}^{test2}). The first one is the configuration the V2 model is based on, and therefore "nominally correct". The second one was used for the later S6b. The latter two are due to intentional test during the science mode by detchar group. Figure 4.1 shows the mismatch of all four configurations.

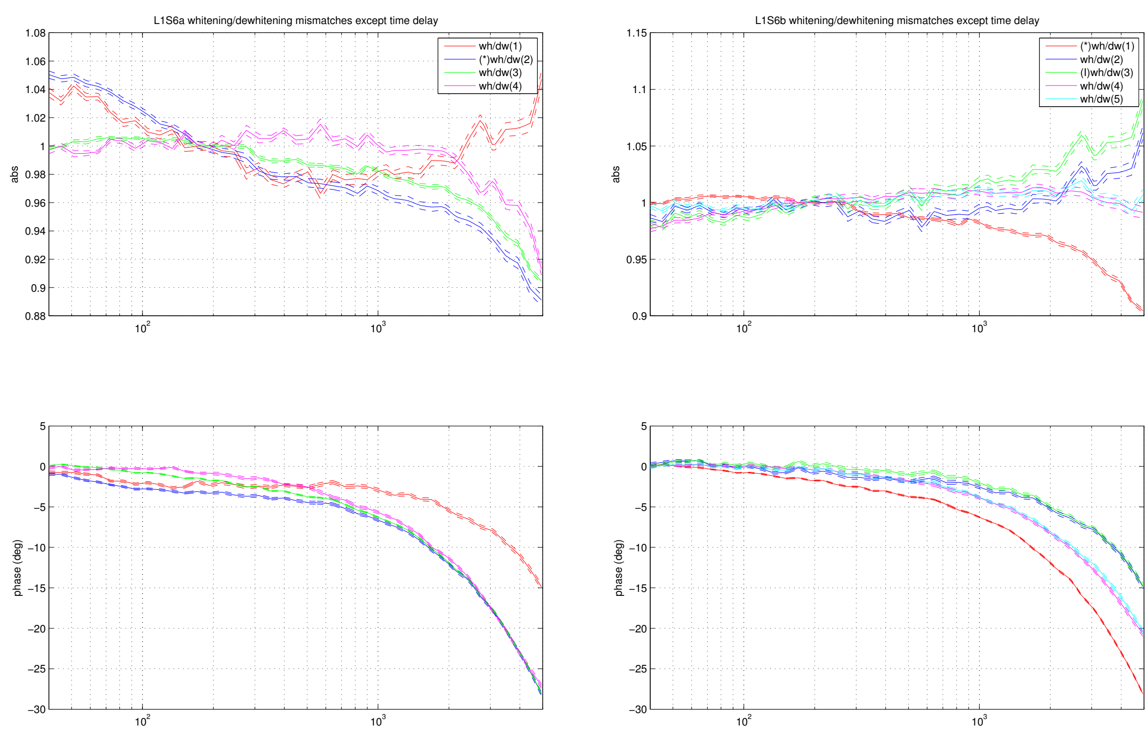

Figure 4.1: L1 sensing systematics due to whitening/dewhitening mismatch in OMC for S6a (left) and S6b (right). Nominally correct configuration and the configuration used in the blind injection are marked by (*) and (I) in the legend.

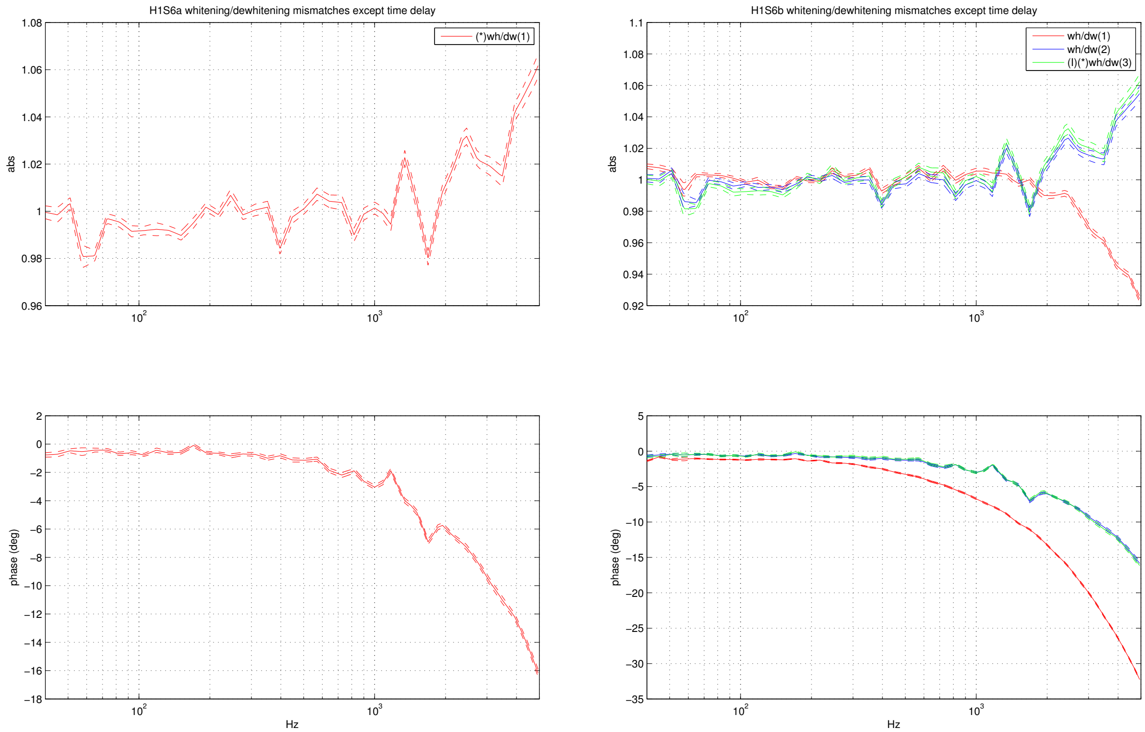

Figure 4.2: H1 sensing systematics due to whitening/dewhitening mismatch in OMC for S6a (left) and S6b (right). Nominally correct configuration and the configuration used in the blind injection are marked by (*) and (I) in the legend.

For H1, there are two configurations: "Nominally correct" one is FM1/FM2/FM3 for both PD1 and PD2 (θ^0_{wh}), and FM1/FM2 for both PD1 and PD2 (θ^{FM12}_{wh}) that was used for a very short period (Fig.4.2).

Note that $|\theta_{wh}|$ shown here are scaled such that $|\theta_{wh}|$=1 at the nominal unity gain frequency, f_{UGF}, of the DARM servo loop. This is because the calibration code tries to dynamically scale the sensing so the OLG is the most correct at this frequency. The error in this scaling is evaluated separately.

Also note that θ_{wh} contains a phase systematic that is proportional to the frequency:

$$\theta_{wh} \equiv |\theta_{wh}| \exp(i\Delta\phi_{wh} - 2\pi i f \tau_{wh}). \tag{4.1}$$

In the phase plot, the time shift is already removed from the mean (green) trace. Table 8shows the time delay of the mismatch for each of the configurations.

L1	$\tau_{wh}^{0} = 16.3\mu$s	$\tau_{wh}^{FM123} = 7.1\mu$s	$\tau_{wh}^{test1} = 11.9\mu$s	$\tau_{wh}^{test2} = 11.4\mu$s
H1	$\tau_{wh}^{0} = 8.8\mu$s	$\tau_{wh}^{FM12} = 18.1\mu$s		

Table 8: List of time delay in whitening/dewhitening mismatches. Positive number means that the true sensing is delayed than the model.

4.1.2 Error in Arm Poles

Version 2 calibration model has two (in the case of L1) or one (H1) parameter representing the corner frequencies of the arm cavities that were simply inherited from S5 model. Any difference between the real corner frequencies and the model parameters should be captured in the OLG residual.

There are three sets of relevant measurements for arm poles after S5 completed. All of the measurements were done by ring down measurement of arm cavities. First one of the arm cavities is locked and then unlocked as fast as possible, and the power of the leakage from inside the cavity is measured and the time constant is obtained by fitting the time series to the exponential decay. The errors associated with the measurements are dependent on the unlocking method. These measurements are shown in Fig.4.3.

Each of the measurements comprises multiple trials, so we have a mean and a standard deviation for each:

$$f_n^{arm} = mean_n^{arm} \pm \sigma_n^{arm} \tag{4.2}$$

where n is either 1, 2 or 3, and arm is either X or Y. The weighted average, weighted one sigma error and the worst case numbers are obtained by

$$\begin{aligned}
f_{wAvg}^{arm} &= \Sigma_n f_n^{arm} w_n^{arm} / \Sigma_n w_n^{arm} && (4.3)\\
\sigma_{wAvg}^{arm} &= 1/\sqrt{\Sigma_n w_n^{arm}} && (4.4)\\
w_n^{arm} &= 1/(\sigma_n^{arm})^2 && (4.5)\\
f_{max}^{arm} &= \max(f_n^{arm} + \sigma_n^{arm}) && (4.6)\\
f_{min}^{arm} &= \min(f_n^{arm} - \sigma_n^{arm}). && (4.7)
\end{aligned}$$

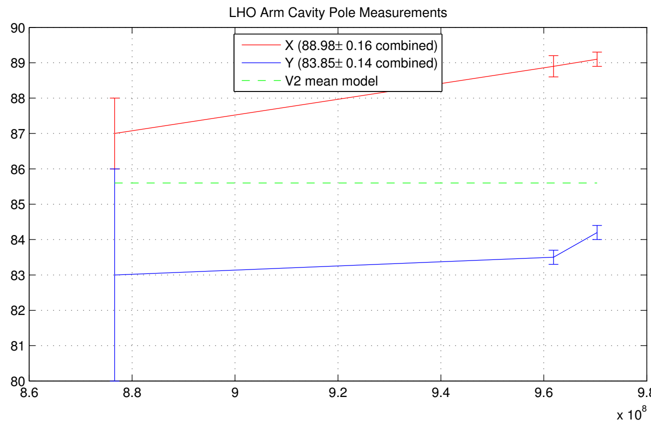

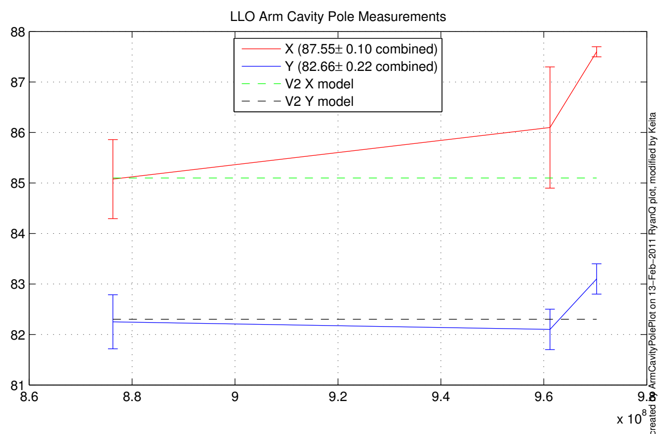

Figure 4.3: Arm pole measurements. L1 model (bottom) uses two parameters (one each per arm) while H1 model (top) uses only one parameter, i.e. the mean pole.

Figure 4.4 shows the ratio of the measurement/V2 sensing function ratio using the measured arm poles. Though the plots show the raw ratio, in the calibration analysis code θ_{arm} is scaled such that $|\theta_{arm}(f_{UGF})| = 1$, just like θ_{wh}.

4.1.3 OMC ADC Clock Timing

Because of a CPU startup problem etc., the timing of the OMC ADC is known to have changed during S6. This has been monitored throughout S6 by injecting a signal generated by arbitrary waveform generator (AWG) into one of the unused OMC ADC channels. To distinguish the timing change of the AWG from that of OMC ADC, the same AWG signal was also monitored by the ADC in the LSC, which works independently of the OMC ADC: If a timing change comes from AWG, both OMC and LSC should see the same change at

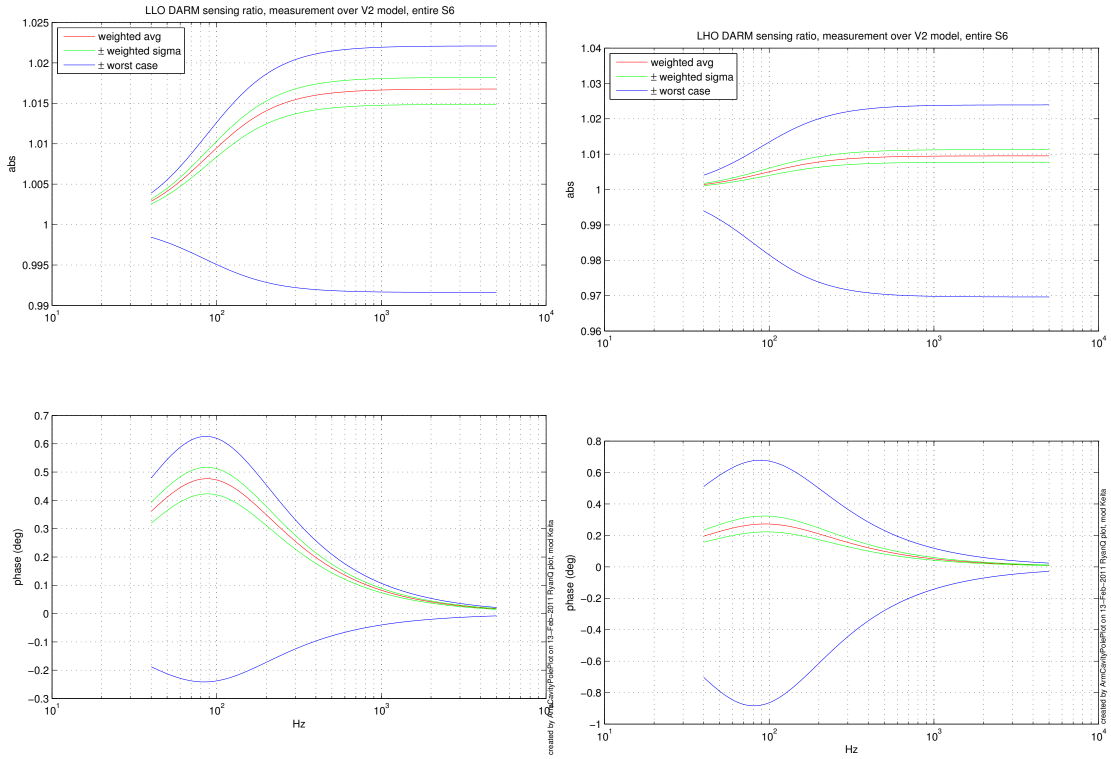

Figure 4.4: Sensing function ratio θ_{arm} using the measured arm poles over V2 model.

the same time.

The timing delay of τ_{ADC} causes the delay of the sensing function, and therefore the advancement of the response function, by that much.

Figure 4.5 shows the OMC ADC timing trend for the entire S6. L1 has seen many distinct timing jumps, but eventually τ_{ADC} settled down to 17 μs delay. Note that there was a large reconfiguration of the timing system at LLO (indicated by a black broken line). H1 has been very stable at 1.2 μs delay except very small percentage of science segments.

4.1.4 Latency Between Two Sensing CPUs

In S6 each LIGO instrument used two CPUs called OM1 and LSC for the sensing function. The analog signal is recorded by ADC and processed by OM1, then passed to LSC for further processing. The latency between these two CPUs is supposed to be 2 clock cycles of OM1 or about 61 μs, however it was not always the case for the issue of the CPU initialization and data hand-off. For S6b, 61 μs was used in the model. For S6a, due to various reasons,

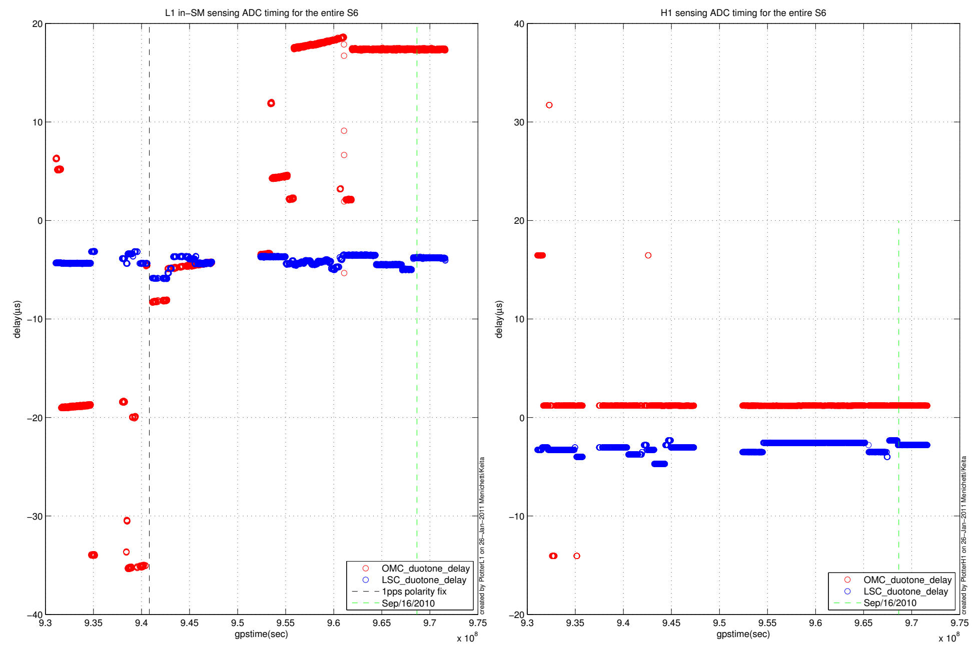

Figure 4.5: ADC timing for L1 (left) and H1 (right) for the entire S6. For L1, several distinct timing jumps happened, and eventually it settled to about 17 μs of delay. H1 OMC ADC has been delayed by 1.2 μs except very small percentage of science segments.

45.8 and 53.4 μs were used for L1 and H1, respectively.

Figure 4.6 shows the OM1-LSC latency difference between the measurement and the V2 model for the entire S6. Positive number means that the reality was delayed than the model suggested.

4.1.5 ETMY Abnormal Resonance in H1

It was found that H1 ETMY has some unknown resonant structures at high kHz frequency range. The EY abnormal resonance effect θ_Y (Fig.4.7, left) is calculated by first by injecting into ETMX and ETMY independently, and then making the DARM actuation effect by taking a ratio $(A_x + A_y)/2A_x$.

For H1, the effect is smaller than 5% for f<2kHz, and since at 1 kHz the amplitude is already 1.018 and the phase -0.07 degrees, we simply assume that it is equal to unity for $f < 1000$. For L1, since the same measurement showed no such anomaly, we assume that $\theta_Y = 1$. Any remaining systematic due to this effect for both of the interferometers should appear in OLG error measurement.

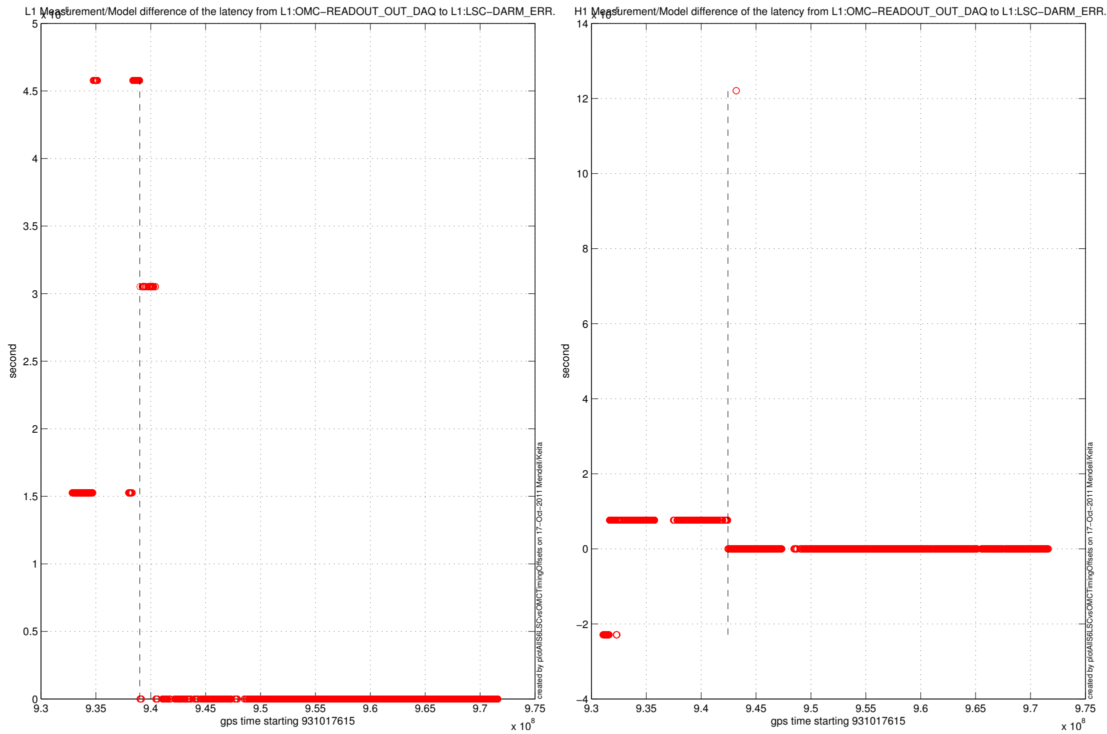

Figure 4.6: OM1-LSC latency difference between the measurement and the model for the entire S6a. Broken line indicates the end of S6a calibration epoch. Positive number means that the reality was delayed than the model suggested.

4.1.6 Mass Deformation

The mass deformation systematic θ_{mass} comes from the fact that the mirror is not a rigid body and therefore deforms according to the actuation force on the magnets. This effect was calculated by finite element analysis (Fig. 4.7, right) assuming that there is no abnormal resonance structure like θ_Y.

For frequency larger than 1kHz, two systematics θ_Y and θ_{mass} should be accounted for in the known part of our best-guess actuation model:

$$A^B_{M0} = A_{M0}\theta_Y\theta_{mass}. \tag{4.8}$$

4.1.7 OLG Residual and Unknown Delay in the Model

In S6 calibration model, there are two systematics the origin of which are not fully known. These are in the actuation model as a buffer so that the OLG model agrees with the mea-

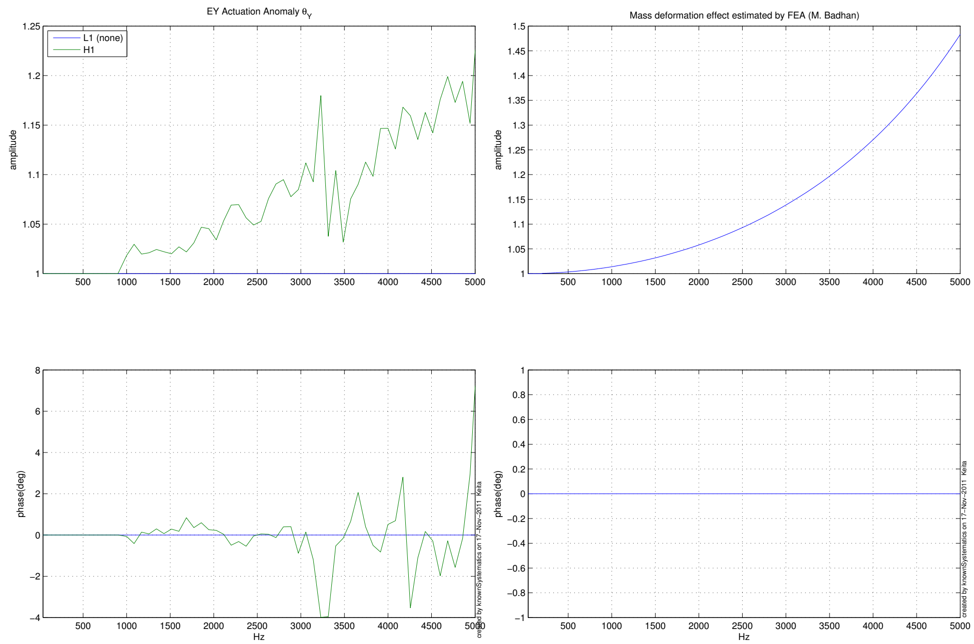

Figure 4.7: EY actuation anomaly systematic θ_Y that is only in H1 (left), and the mass deformation systematic θ_{mass} (right). Smaller peaks/valleys of 2% 1 degree level in θ_Y are the measurement noise, but larger structures in amplitude and phase for $f > 3000$ Hz are real resonance.

surement:

$$G \sim G_M = G_{initial} Res_M e^{-2\pi i f \tau_M} \tag{4.9}$$

where $G_{initial}$ is the open loop transfer function with only known modeled elements. In this expression, a phase systematic that is proportional to the frequency is parametrized as an ad-hoc time delay τ_M and the rest is modeled as a function called the OLG residual (Res_M). These two systematics are supposed to represent the combined effect of all unknown and known systematic that are not explicitly put in the model. True unknown systematics are derived from Res_M and τ_M by removing all known systematics.

OLG residual and unknown time delay in the model were generated by a fit of OLG measurement G over the initial model. As such, OLG residual does capture the overall trend of the systematics, but sharp features like resonant structures of θ_Y are not captured. Sometimes the fit was done for the mean of several measurements (S6a), thus the OLG residual does not necessarily capture any specific hardware configuration.

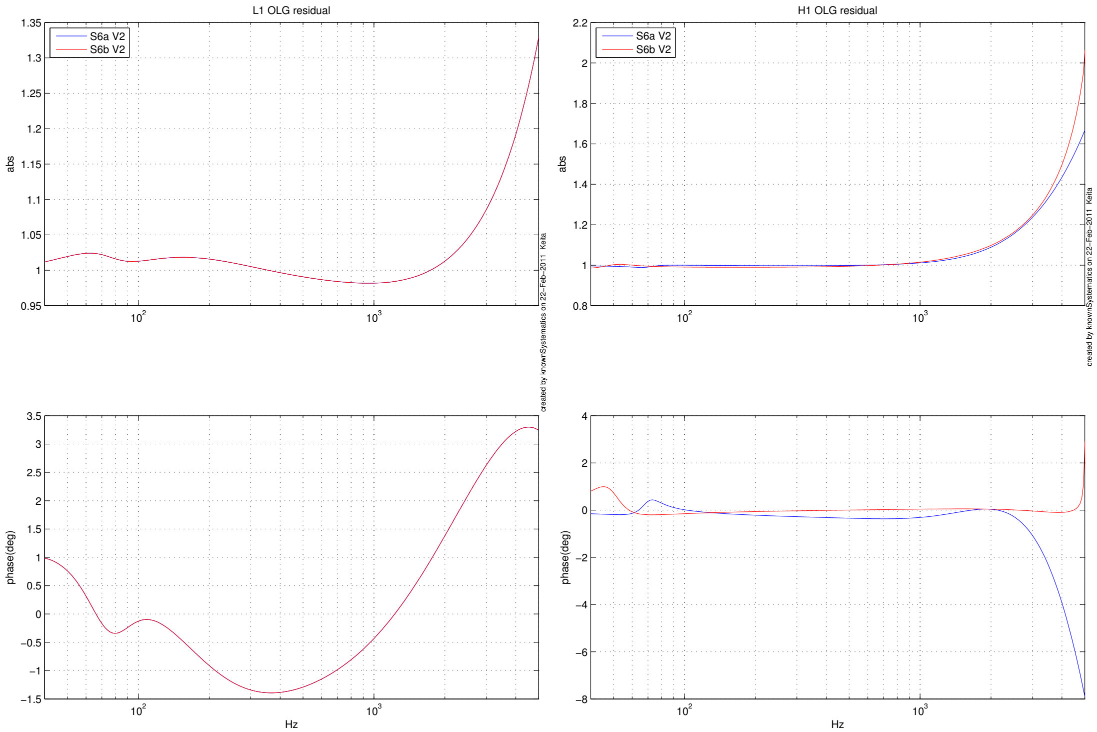

Figure 4.8: OLG residual of L1 (left) and H1 (right). For L1, S6a OLG residual is identical with S6b. The difference between S6a and S6b for H1 is the quality of the fit.

Figure 4.8 shows the OLG residual for L1 and H1. Note that L1 has a single OLG residual that is used for the entire S6a, while H1 has two. This is not due to physical change in the H1 instrument, but rather due to an improvement in the fit technique. In S6a, the H1 fit was confused by the high frequency phase structure of θ_Y that was out of LIGO calibration band of [40, 5000] Hz, skewing both the amplitude and the phase for $f > 3$ kHz. This was much improved in S6b.

4.1.8 OLG Mismatch

Even with the OLG residual in the model, there might still be a systematic error in the OLG model partly due to a limited S/N for any of the measurements used to generate the model, inaccuracy in the fit (e.g. H1 S6a) and partly due to the fact that the LIGO instruments are sometimes in configurations other than nominally correct one. This error was evaluated regularly throughout the S6 run by measuring the open loop transfer function.

Figures 4.9 and 4.10 show the ratio of the measurement over the V2 model for S6a and

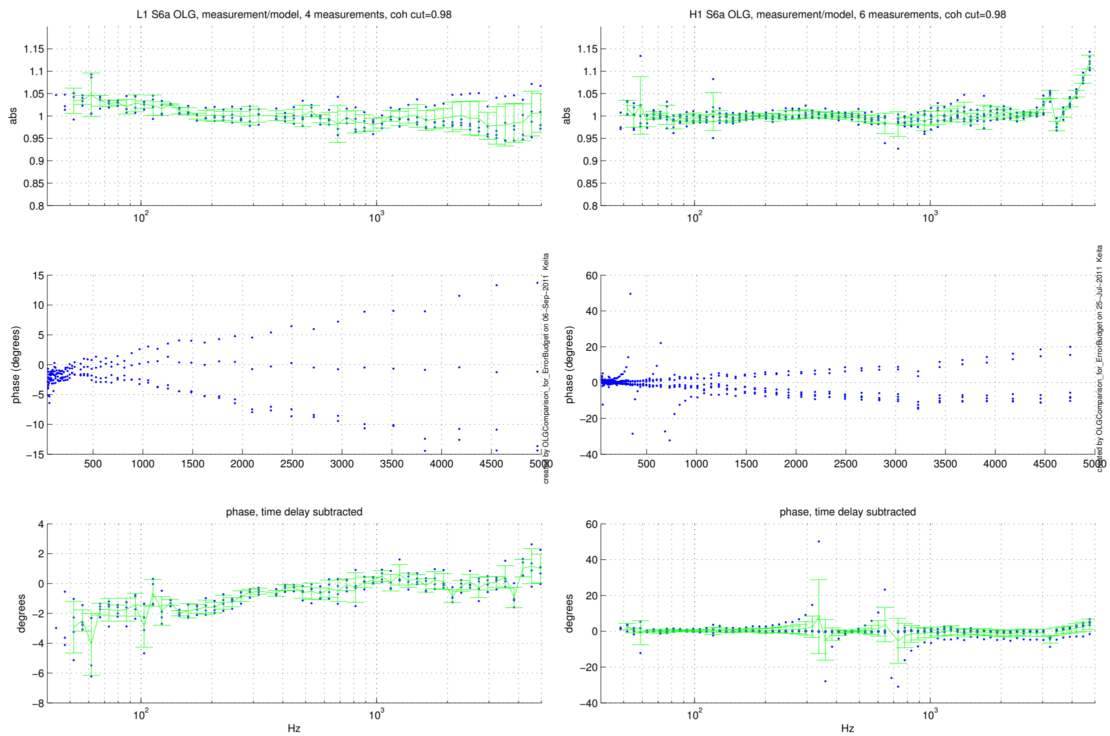

Figure 4.9: Ratio of the open loop transfer function measurements over the V2 model for S6a.

S6b, respectively. All measurements are scaled such that the discrepancy becomes minimal at the unity gain frequency to factor out small differences in the optical gain due to alignment of the optics, thermal lensing in the ITMs and any incompleteness in the dynamic gain scaling code of the LIGO control system. Note that there are many distinctive phase systematics that are proportional to the frequency in the middle plots. This is mostly the latency jump in the loop due to the CPU initialization issue etc., mainly at the end stations, for both IFOs (another reason is the whitening configuration change in L1, which is discussed later). There is little uncertainty in latency mismatches, so it is convenient to divide η_G into two parts, i.e. the systematic except the latency mismatch and the latency mismatch:

$$\eta_G = \theta_G \exp(2i\pi f \tau_G) \tag{4.10}$$

$$\theta_G = \mathrm{abs}(\eta_G) \times \exp(i\Delta\phi_G). \tag{4.11}$$

In the bottom plots, this latency mismatch was subtracted from the phase.

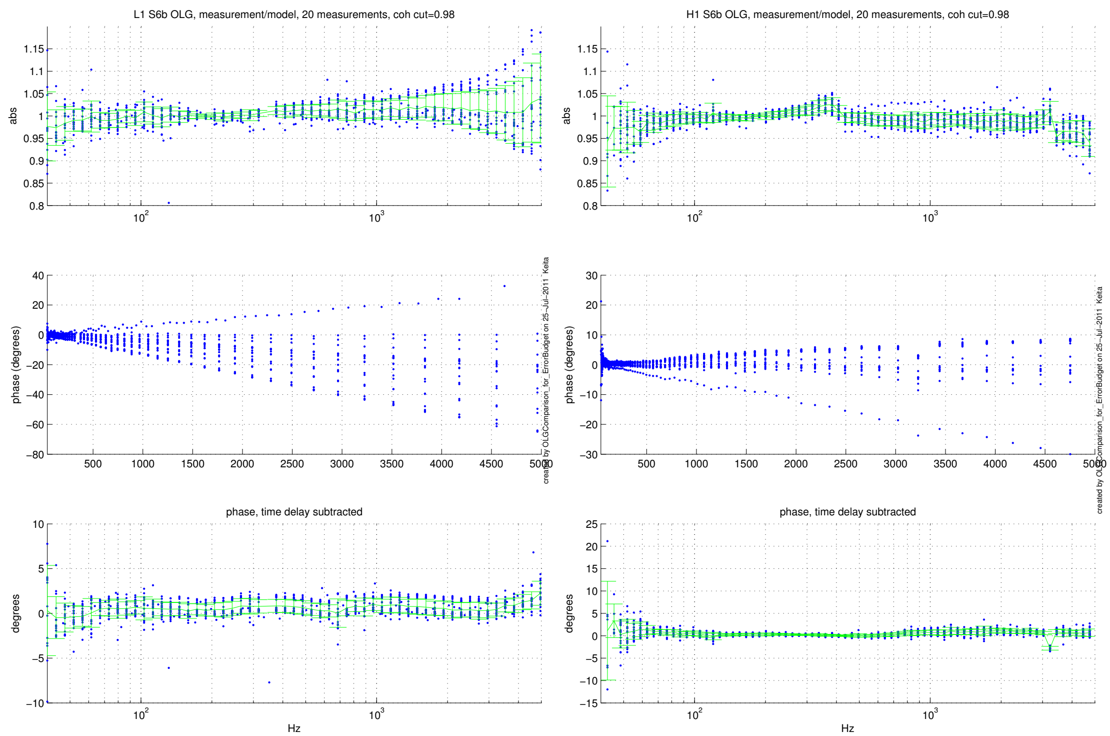

Figure 4.10: Ratio of the open loop transfer function measurement over V2 model in the second calibration epoch for L1 (left) and H1 (right). Error bars show the standard deviation. For L1 we cannot use this as is for the assessment of the true statistical error inherent in the OLG measurements, as two different configurations are present in the measurement.

Even after subtracting the latency changes, however, because of the fact that different whitening/dewhitening configurations are present in the OLG measurements, we cannot use the measurement over the V2 model as is to make a correct assessment of the statistical error in the OLG measurements. One could obtain an error for a specific configuration by only using the measurements in that configuration. However, in doing so, the number of measurements is going to be limited (or none for some of the configuration). Instead, assuming that we know all the differences between different configurations, we can propagate an error in any configuration into "nominally correct" one by building a configuration-specific open loop transfer function model.

True mismatch in "nominally correct" configuration Figure 4.12 on the left shows the L1 OLG measurement data divided by configuration-specific OLG model. For "nominally correct" configuration, the measurement was divided by V2 model G_M. For the measure-

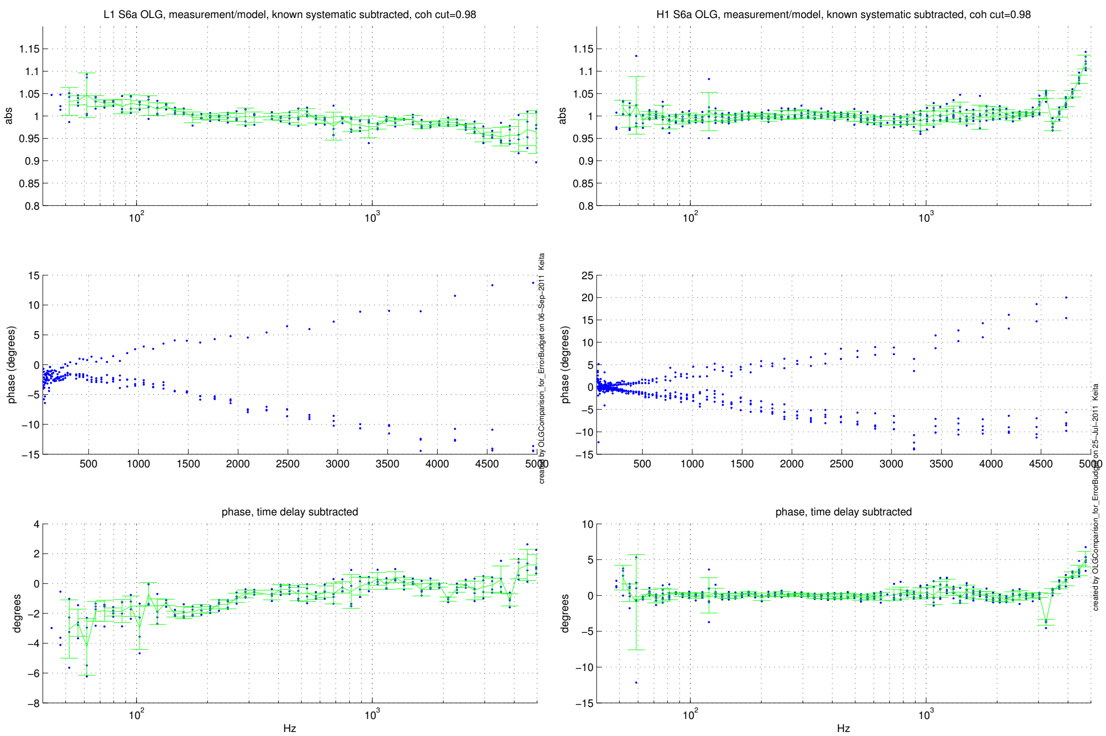

Figure 4.11: S6a OLG measurements divided by the configuration-specific OLG models for L1 (left) and H1 (right).

ments made with θ_{wh}^{FM123} configuration for example, we used $G_M\theta_{wh}^{FM123}/\theta_{wh}^0$ instead. This shows how the OLG mismatch would have looked if all measurements were done with nominally configuration, and as such this is a true measure of the OLG mismatch for the nominally correct configuration.

The top and the bottom represents the ratio of the measured and the V2 model open loop transfer function in amplitude and phase except the latency mismatch for the nominally correct configuration, i.e. abs(θ_G^0) and $\angle\theta_M^0$:

$$
\begin{aligned}
G^0 &= G_M^0|\theta_G^0| \times \exp i(\angle\theta_M^0 + 2\pi f\tau_G) && (4.12)\\
|\theta_G^0| &= <|\theta_G^0|> \pm \mathrm{std}|\theta_G^0| && (4.13)\\
\angle\theta_G^0 &= <\angle\theta_G^0> \pm \mathrm{std}(\angle\theta_G^0) && (4.14)
\end{aligned}
$$

where <> and std() means the mean and the standard deviation. Uncertainty in latency

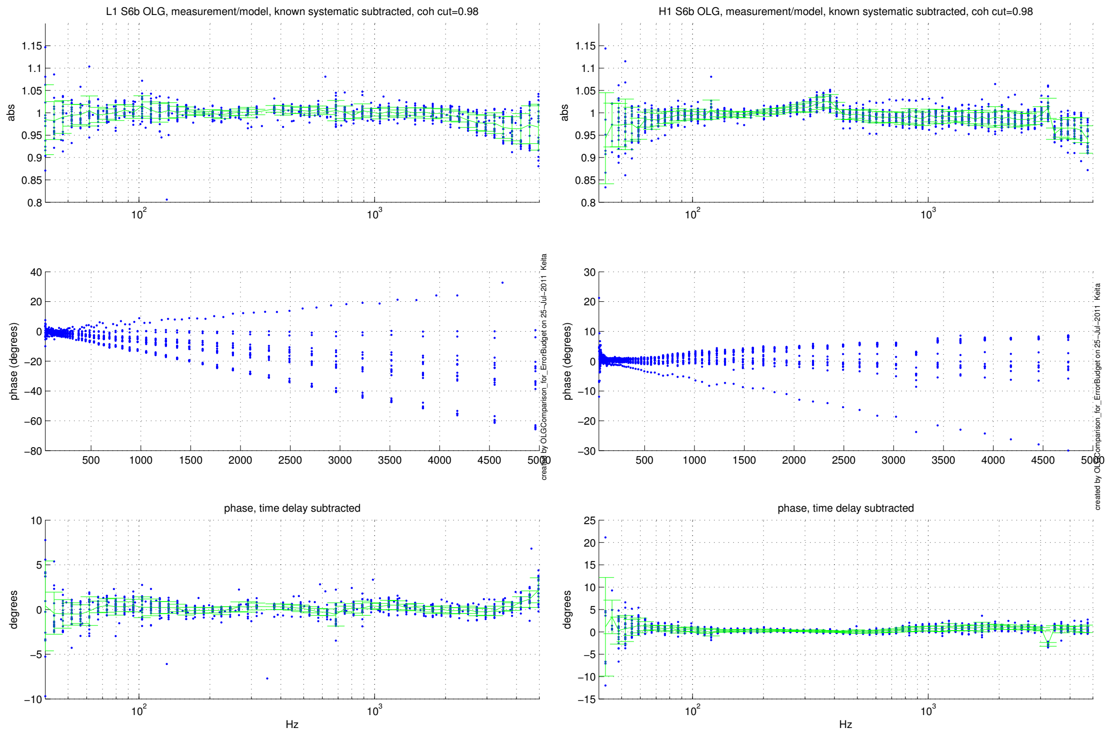

Figure 4.12: S6b OLG measurements divided by the configuration-specific OLG models for L1 (left). Error bars represent the standard deviations. H1 data (right) is the same as the one in Fig.4.10. These represent the open loop transfer function error of V2 model η_G only for a nominally correct configuration. Note that these plots don't include the correction for the H1 ETMY anomaly in the actuation.

part τ_M^0 is so small that it's ignored.

The latency part at any GPS time is obtained by a single measurement, either from an OLG measurement close enough to the gps time of interest (see 4.1.9 and Fig.4.13), or from the calibration factors.

The error of the OLG mismatch measurement is in general the smallest in [80 1000] Hz band. As you go lower in frequency, both the instrument noise and the amplitude of the OLG become larger very quickly, resulting in a smaller coherence of the measurement. On the opposite side of the LIGO frequency band, as you go higher than 1000 Hz, though the instrument noise and the OLG amplitude stays reasonable, it becomes more and more difficult to drive the mirrors with a good S/N because of $1/f^2$ dependence, again making it very difficult to obtain a good coherence.

True mismatch in other configurations For any configuration other than the nominally correct one, the open loop transfer function error is composed of two elements, i.e. the error of an unknown origin that is represented by Fig.4.12 ($|\eta_G^0|$ and $\Delta\phi_G^0$) and a known systematic due to configuration change, e.g.

$$\left|\theta_G^{FM123}\right| = \left|\theta_G^0\right| \times \left|\theta_{wh}^{FM123}/\theta_{wh}^0\right| \tag{4.15}$$

$$\angle\theta_G^{FM123} = \angle\theta_G^0 + \Delta\phi_{wh}^{FM123} - \Delta\phi_{wh}^0. \tag{4.16}$$

Again, the latency mismatch should be obtained from the near-by OLG measurement or from the factor analysis.

4.1.9 Latency Mismatch

Latency mismatch τ_G is the time constant of the phase systematic that is linear to the frequency derived from OLG measurements divided by the V2 model. Figure 4.13 shows the latency mismatch τ_G obtained from the OLG measurement and V2 model as a function of GPS time. Other timing parameters are also shown in the plot: Model timing parameter τ_M representing an ad-hoc delay which is placed in the actuation, ADC timing delay τ_{ADC}, OM1-LSC latency error τ_{CPU} which is the difference of the true OM1-LSC latency and the latency number in the model, and whitening/dewhitening mismatch delay τ_{wh}. See Section 7 for the details of the timing analysis.

4.1.10 Unknown Residual in OLG

As we learned, the combination of OLG residual, ad-hoc delay and OLG mismatch represents the effect of all known and unknown systematic. Since we do not know if this residual is in the sensing or not, as a conservative measure we fold this into the potential error in the sensing. The timing shift part of this was already explained in the previous section, so let's now look at the amplitude and the phase systematic that is not a time delay.

All actuation systematics as well as the most likely value of the arm pole error are simply

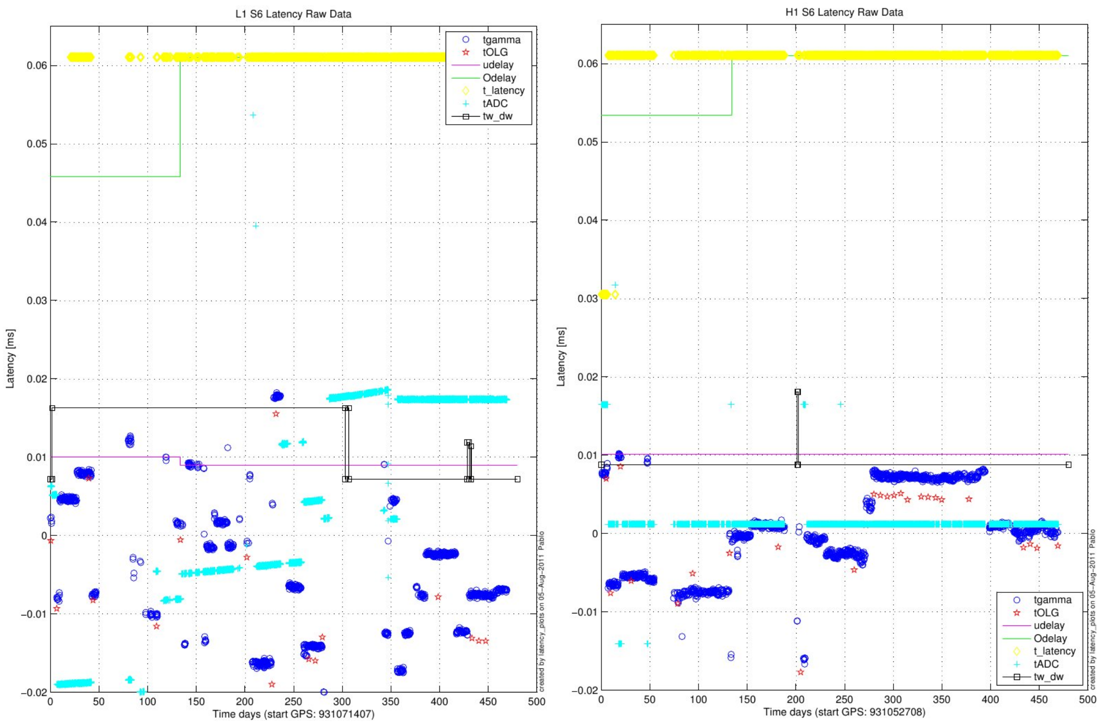

Figure 4.13: Latency mismatch τ_G obtained from the ratio of OLG measurement over the V2 OLG model (red) together with other timing-related parameters. Negative τ_G means that the model is advanced, and needs more delay in order for the model to become consistent with the measurement. Note the notation difference here: τ_G, τ_M, τ_{ADC} and τ_{wh} in the text are written as t_{OLG}, $udelay$, t_{ADC} and t_{wh-dw} in the plot. Also, τ_{CPU} in the text is represented by $t_{latency} - Odelay$ in the plot. Another measure of latency is obtained from the analysis of the calibration line that is constantly injected to the coil actuator, which is represented by t_{gamma} in the plot.

removed from the OLG residual. Since OLG residual was constructed using "nominally correct" whitening filter configuration, these sensing systematics should also be removed from the OLG residual to obtain the unknown part:

$$Res_M^B \quad = \quad \frac{Res_M \exp(-2\pi i f \tau_{wh}^0).}{\theta_{wh}^0 \theta_{arm} \theta_{YX} \theta_{mass}} \tag{4.17}$$

This represents the unknown part of the OLG residual. Note the delay parameter in the numerator that was put in to remove the timing part from θ_{wh}^0.

The product $Res_M^B \times \theta_{OLG}^0$ represents the true unknown residual in the OLG. Figure 4.14 shows Res_M^B together with $Res_M^B \times \theta_{OLG}^0$.

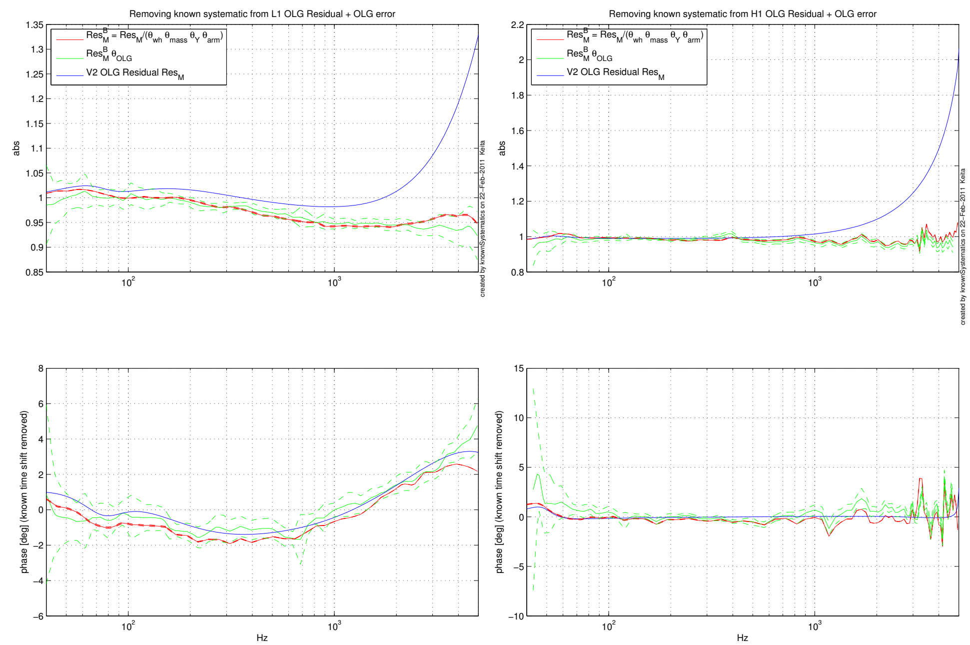

Figure 4.14: Red traces represent the OLG residual after all known systematics are removed for "nominally correct" configuration in S6b for L1 (left) and H1 (right). Only the arm pole error bar is considered for the error bar of the red traces. Blue traces are the V2 OLG residual model. Green traces are the product of the red traces and the OLG mismatch θ_{OLG}. This represent the truly unknown residual in the OLG, and the error bar is dominated by that of θ_{OLG}.

4.2 Combining Errors for Sensing

The error in the sensing function except the overall factor comprises the known systematic in the sensing, the ADC timing, OMC-LSC CPU latency, and the unknown residual in the OLG. This is written by the known sensing systematic η_C^{known} and unknown systematic uncertainty η_C^U as

$$C \equiv C_M \eta_C^{known} \eta_C^U \tag{4.18}$$

$$\eta_C^{known} \equiv \theta_{wh}(f)\theta_{arm}(f) \exp\left[-2i\pi f(\tau_{ADC} + \tau_{CPU})\right] \tag{4.19}$$

$$= |\theta_{wh}(f)\theta_{arm}(f)| \exp i\left[\Delta\phi_{wh} + \Delta\theta_{arm} - 2\pi f(\tau_{wh} + \tau_{ADC} + \tau_{CPU})\right] \tag{4.20}$$

$$\eta_C^U \equiv [1, Res_M^B \theta_{OLG}^0]. \tag{4.21}$$

The last equation is worth an explanation. Since we don't know if the unknown residual

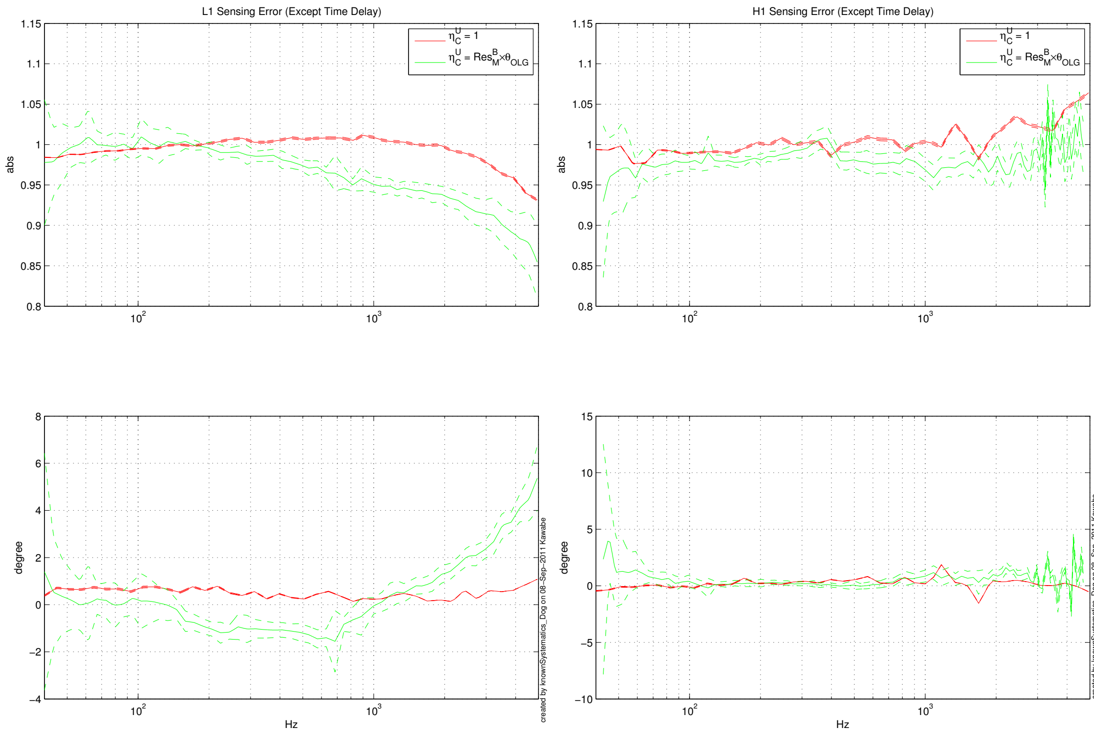

Figure 4.15: Sensing Errors at the end of S6b starting 14/Sep/2010 corresponding to the case where all (green) or none (red) of the true unknown mismatch in the OLG are in the sensing. Note that the known timing delay ($\tau_{wh} + \tau_{ADC} + \tau_{CPU}$=24.5 μs for L1 and 10.0 μs for H1) are removed from the phase plot.

in the OLG ($Res_M^B \theta_{OLG}^0$) comes from the sensing, this is folded into the systematic error of the sensing. We consider two extrema cases where either none or all of $Res_M^B \theta_{OLG}^0$ is in the sensing ($\eta_C^U = 1$ or $Res_M^B \theta_{OLG}^0$).

Latency mismatch is not explicitly put into the sensing error, as the timing is handled separately later.

The sensing function error budget is shown in Fig.4.15. for the sensing error budget using the above equations.

4.3 Combining Errors for Closed Loop Response

Since the response function is proportional to the close loop response $1+G$, we need to propagate the error in G to $1+G$:

$$\begin{aligned}
\eta_{(1+G)} &= \frac{1+G_M\theta_{OLG}\exp(2i\pi f\tau_G)}{1+G_M} \\
&= |\eta_{(1+G)}|\times\exp(i\Delta\phi_{(1+G)}) && (4.22) \\
<|\eta_{(1+G)}|> &= \left|\frac{1+G_M<|\theta_{OLG}|>\exp i(<\Delta\phi_{OLG}>+2\pi f\tau_G)}{1+G_M}\right| && (4.23) \\
\mathrm{std}(|\eta_{(1+G)}|) &= \frac{|G_M|\sqrt{\mathrm{std}(|\theta_{OLG}|)^2\cos^2\epsilon+<|\theta_{OLG}|>^2\,\mathrm{std}(\Delta\phi_{OLG})^2\sin^2\epsilon}}{|1+G_M|} && (4.24) \\
\mathrm{std}(\Delta\phi_{(1+G)}) &= \frac{|G_M|\sqrt{\mathrm{std}(|\theta_{OLG}|)^2\sin^2\epsilon+<|\theta_{OLG}|>^2\,\mathrm{std}(\Delta\phi_{OLG})^2\cos^2\epsilon}}{|1+G_M<|\theta_{OLG}|>\exp i(<\Delta\phi_{OLG}>+2\pi f\tau_G)|} && (4.25)
\end{aligned}$$

where $<>$ and std() represent the mean and the one-sigma level error bar corresponding to the standard deviation of the open loop transfer function error, and ϵ is the angle between $1+G_M<|\theta_{OLG}|>\exp i(2i\pi f\tau_G)$ and $G_M<\theta_{OLG}>\exp(2i\pi f\tau_G)$. For a full derivation, see Sec.9.1.

Figure 4.16 shows $\eta_{(1+G)}$ for the last part of S6b: θ_{wh}^{FM123} configuration with $\tau_G=-13.3\mu$s for L1, and θ_{wh}^{0} configuration with $\tau_G=-1.6\mu$s for H1.

4.4 Combining Errors for Response Function

Now we combine the error of the sensing and the closed loop response to obtain an error budget of the response function. For notational simplicity, we ignore the overall timing factor

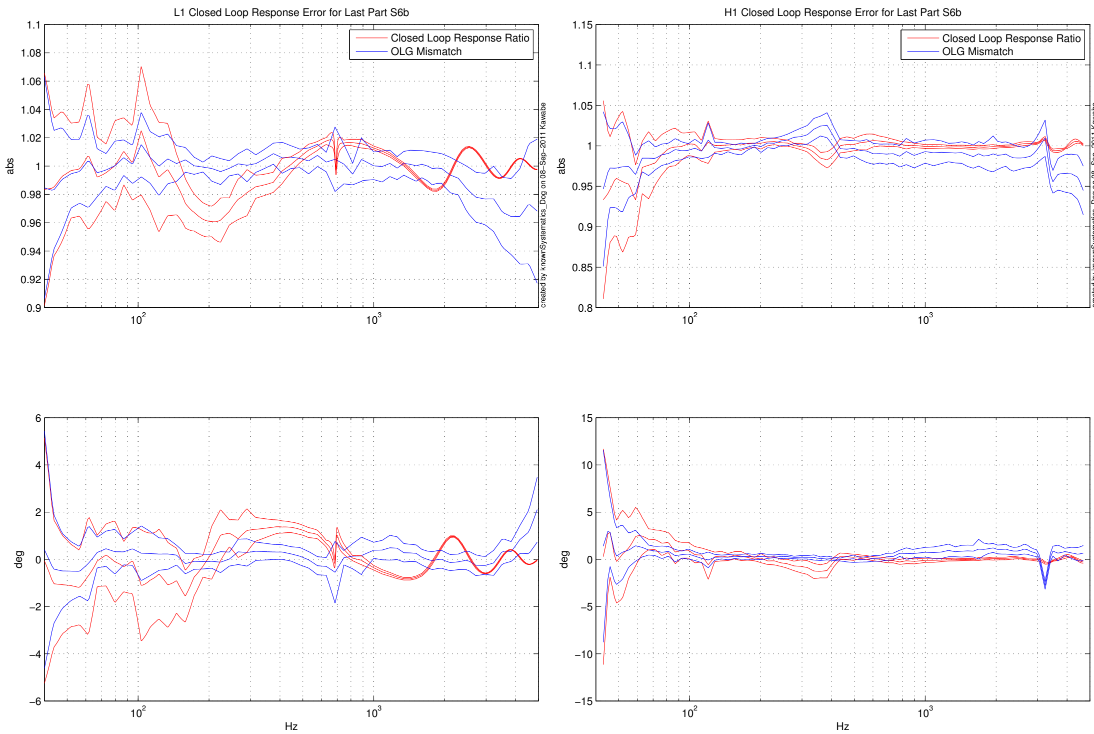

Figure 4.16: Closed loop response error $\eta_{(1+G)}$ example (red) for the last part of S6b starting Sep/14/2010. The error bar represents the standard deviation of the OLG mismatch (η_G, blue) propagated to $\eta_{(1+G)}$.

in the form of $\exp 2i\pi f\tau$, and calculate the timing error separately later in Section 7.

$$\begin{aligned}
\eta_R(\eta_C^U = 1) &= \frac{\eta_{(1+G)}}{\eta_C^{known}} \\
&= \frac{1 + G_M\theta_{OLG}e^{2i\pi f\tau_G}}{(1+G_M)\theta_{wh}\theta_{arm}} && (4.26) \\
\eta_R(\eta_C^U = Res_M^B\theta_{OLG}^0) &= \frac{\eta_{(1+G)}}{\eta_C^{known}Res_M^B\theta_{OLG}^0} && (4.27) \\
&= \frac{1 + G_M\theta_{OLG}e^{2i\pi f\tau_G}}{(1+G_M)\theta_{wh}\theta_{arm}\frac{Res_M}{\theta_{wh}^0\theta_{YX}\theta_{mass}\theta_{arm}}\theta_{OLG}^0} && (4.28) \\
&= \frac{G_M\theta_{YX}\theta_{mass}}{(1+G_M)Res_M} \times \frac{1 + G_M\theta_{OLG}e^{2i\pi f\tau_G}}{G_M\theta_{OLG}e^{2i\pi f\tau_G}} && (4.29) \\
&= \frac{G_M\theta_{YX}\theta_{mass}}{(1+G_M)Res_M} \times \frac{1+G}{G}. && (4.30)
\end{aligned}$$

We used the relation $\theta_G = \theta_G^0\theta_{wh}e^{-2if(\tau_{wh}^0 - \tau_{wh})}/\theta_{wh}^0$ (again note the omission of overall timing factor in the equations), and substituted $G_M\theta_{OLG}e^{2i\pi f\tau_G}$ with G to obtain the last expression.

For a reasonable error evaluation, two error bands corresponding to one sigma error were calculated first, i.e. one with $\eta_C^U = 1$ and another with $\eta_C^U = Res_M^B \theta_{OLG}$. The first case is simple enough as there is no correlation between the denominator and the numerator:

$$\left|\eta_R^{\pm}(\eta_C^U = 1)\right| = \frac{< |\eta_{(1+G)}| >}{< \left|\eta_C^{known}\right| >} \left(1 \pm \sqrt{\frac{\text{sigma}\left(|\eta_{(1+G)}|\right)^2}{< |\eta_{(1+G)}| >^2} + \frac{\text{sigma}\left(\left|\eta_C^{known}\right|\right)^2}{< \left|\eta_C^{known}\right| >^2}}\right). \tag{4.31}$$

For the second case, the error bar of G in $(1+G)/G$ should be calculated as shown in Section 9.2.

$$\left|\eta_R^{\pm}(\eta_C^U = Res_M^B \theta_{OLG})\right| = \left|\frac{\eta_{(1+G)}}{\eta_C^{known} Res_M^B \theta_{OLG}}\right| \left(1 \pm \frac{\text{std}\left(\left|\frac{1+G}{G}\right|\right)}{\left\langle\left|\frac{1+G}{G}\right|\right\rangle}\right) \tag{4.32}$$

There are no error bars per se in θ_{YX} and θ_{mass}, as any error is in effect included in θ_{OLG}.

As a total error bar, we simply choose the maxima and minima of the four boundary numbers,

$$\begin{aligned}
\left|\eta_R^{+}(\text{total})\right| &= \max\left(\left|\eta_R^{\pm}(\eta_C^U = 1)\right|, \left|\eta_R^{\pm}(\eta_C^U = Res_M^B \theta_{OLG})\right|\right) \\
\left|\eta_R^{-}(\text{total})\right| &= \min\left(\left|\eta_R^{\pm}(\eta_C^U = 1)\right|, \left|\eta_R^{\pm}(\eta_C^U = Res_M^B \theta_{OLG})\right|\right).
\end{aligned}$$

For convenience we also define the mean number and the error bar corresponding to the standard deviation as

$$< |\eta_R(\text{total})| > = \frac{\left|\eta_R^{+}(\text{total})\right| + \left|\eta_R^{-}(\text{total})\right|}{2} \tag{4.33}$$

$$|\eta_R(\text{total})| = < |\eta_R(\text{total})| > \pm \frac{\left|\eta_R^{+}(\text{total})\right| - \left|\eta_R^{-}(\text{total})\right|}{2}. \tag{4.34}$$

One can obtain the phase mean number and the error bar exactly in the same way.

Figure 4.17 shows the response function error $|\eta_R(\text{total})|$ and angle$(\eta_R(\text{total}))$ for the

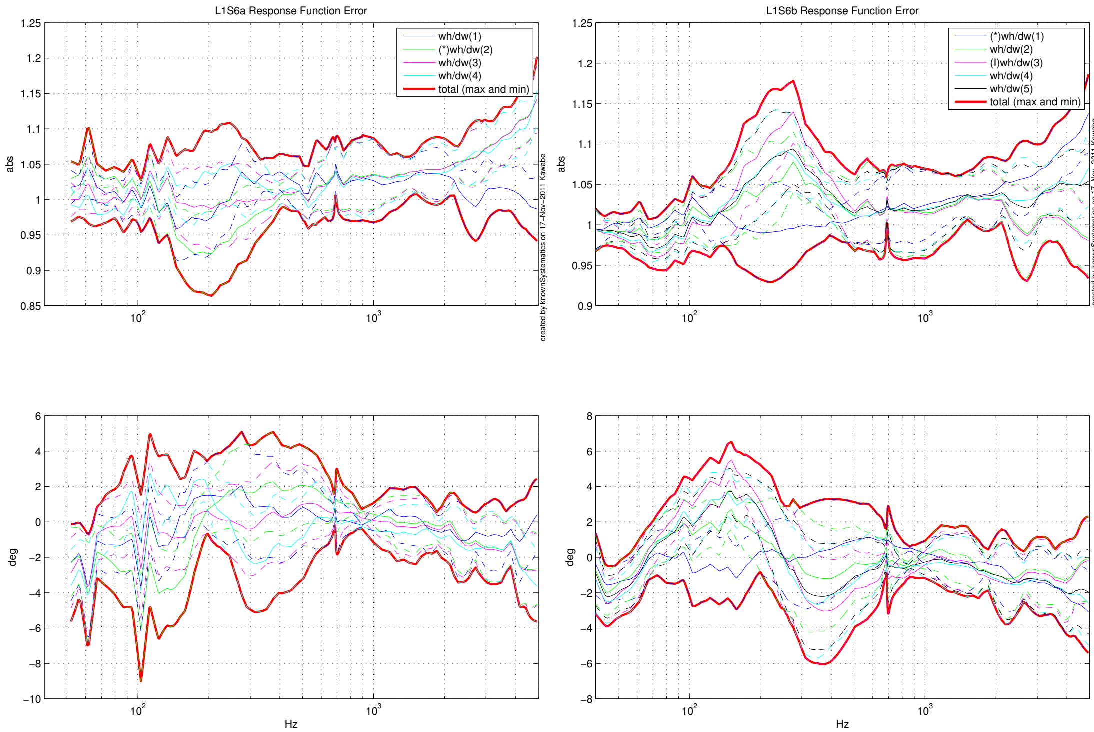

Figure 4.17: Response function error $|\eta_R|$ and angle(η_R) except the time delay for L1. Amplitude larger than 1 means that the signal calibrated by V2 calibration is smaller than it should be. Positive phase means that the signal calibrated by V2 calibration is delayed than it should be. See also Table 10, the time table of all configurations used in S6.

last part of S6b. To stay on the safer side, we recommend that the analysis group use $\pm\max(|\eta_R^+(\text{total})|, |\eta_R^-(\text{total})|)$ and $\pm\max(|\Delta\phi_R^+|, |\Delta\phi_R^-|)$ as the amplitude and the phase error. A summary list of the amplitude and the phase error for several frequency bands was calculated this way.

5 Calibration Factor Error

Due to the fact that only a finite time integration is used to calculate the calibration factor, there is always an uncertainty associated with a measurement noise. Since the factor generation is in the time domain data generation code, and since all analysis groups use the time domain data, the calibration factor error for frequency domain calibration was not included in the error budget of this document. However, just for completeness the magnitude of this noise is described here.

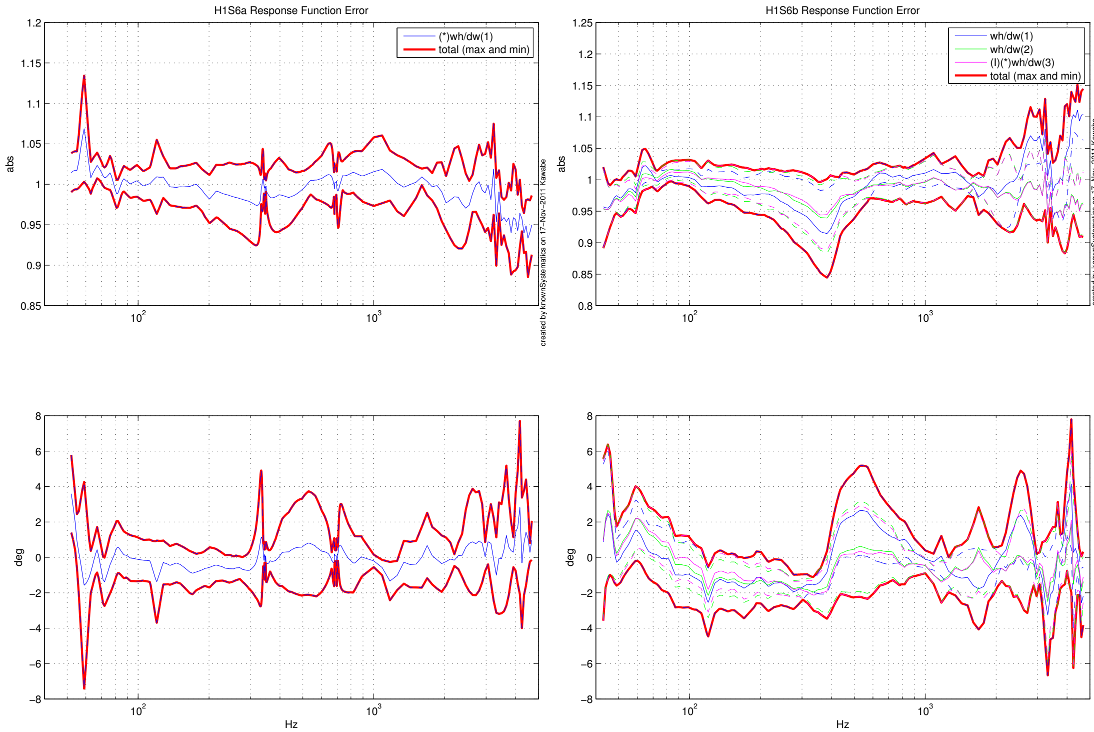

Figure 4.18: Response function error $|\eta_R|$ and angle(η_R) except the time delay for H1. See also Table 10, the time table of all configurations used in S6.

The calibration factor error was evaluated from the imaginary part of γ_M which should be dominated by Gaussian noise. Using the data produced by the time domain calibration code, one sigma level fractional error was about 0.5%:

$$\gamma \sim \gamma_M(1 \pm \delta\eta_\gamma) \tag{5.1}$$

$$\delta\eta_\gamma = 0.5\%. \tag{5.2}$$

Putting the above and $\gamma_M = \eta_G = \eta_C = 1$ into Eq.2.1 we obtain

$$R = \frac{1 + (1 \pm \delta\eta_\gamma)G_M}{(1 \pm \delta\eta_\gamma)C_M} \tag{5.3}$$

$$\eta_R = \frac{1 + (1 \pm \delta\eta_\gamma)G_M}{(1 \pm \delta\eta_\gamma)C_M} \times \frac{1}{R_M}. \tag{5.4}$$

Figures 5.1-5.2 show the uncertainty corresponding to one sigma level errors (i.e. 0.5%)

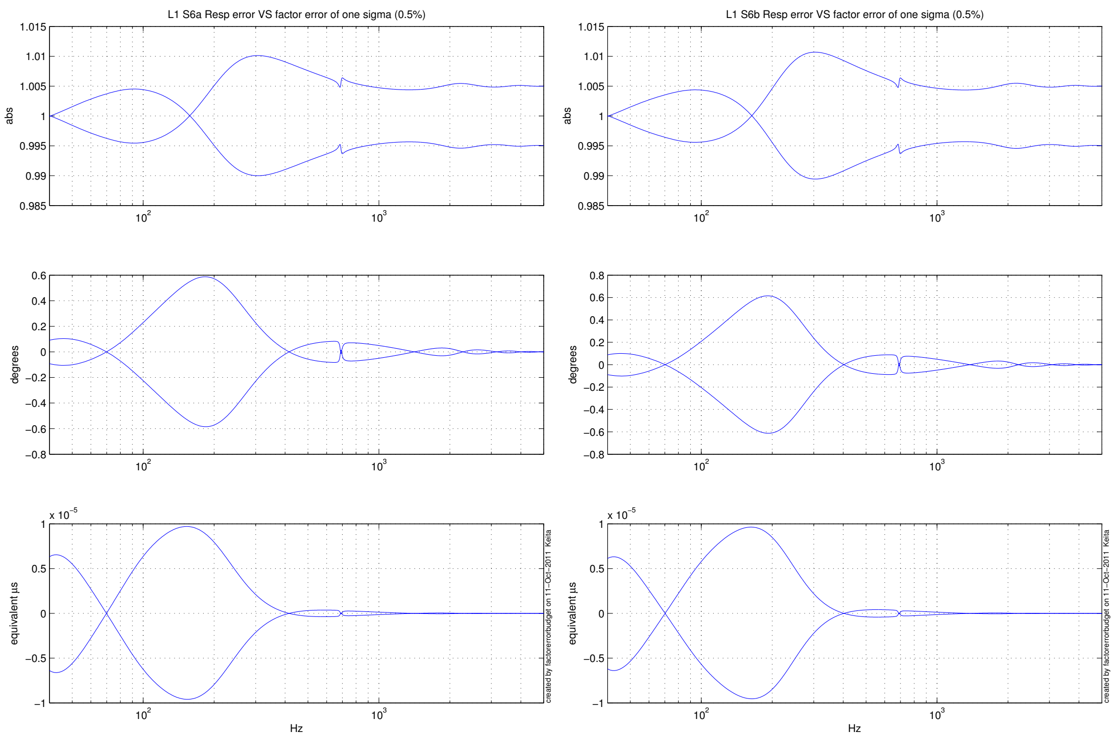

Figure 5.1: L1 response uncertainty VS factor uncertainty.

into Eq.5.4. Note that the phase error caused by the factor error becomes small when the phase angle of G_M is close to $(n + 1/2)\pi$ where n is an integer.

6 Inflating H1 error for [3000, 4000] Hz band.

Though our error analysis fully incorporates the measured H1 EY actuation anomaly θ_Y (Fig.4.7), a special cate has to be taken for a frequency band of [3000, 4000] Hz where some peaks/valleys were observed. Because the frequency resolution of our measurement for θ_Y is finite, we cannot guarantee that the measured θ_Y correctly captured the exact peaks and valleys. Even though this is in the actuation, this could skew our estimate of the response function via the closed loop response. Since we cannot accurately assess the error at around

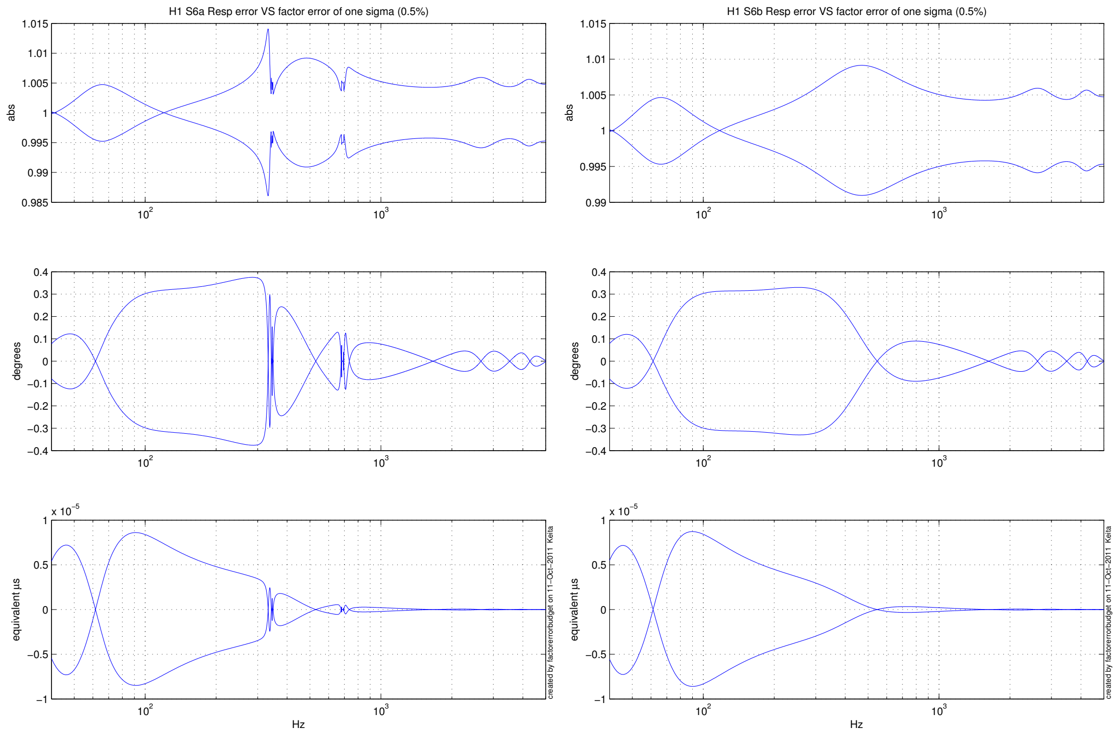

Figure 5.2: H1 response uncertainty VS factor uncertainty.

the true peaks/valleys without any new measurements, we'll give an inflated error for the entire band of [3000, 4000] Hz with some very generous assumptions.

Since the observed resonances in Fig.4.7 are with relatively low Q, it seems safe to assume that true θ_Y cannot be outside of [0.5, 2] range in amplitude. Since we are not attempting a fine grained analysis, we ignore the fact that V2 model incoorporates the overall trend of θ_Y, and simply state that the V2 open loop transfer function model could be in [0.5, 2] range in amplitude. To stay on a safer side, we also assume that the phase error could be any number.

Since we know that this is in the actuation, the error in the response function is thus obtained by

$$\frac{1 + a_Y e^{i\phi_Y} G_M}{1 + G_M} \tag{6.1}$$

where a_Y is the amplitude error of V2 model due to θ_Y and ϕ_Y is the phase. We calculated the amplitude and phase of this quantity over $a_Y = [0.5, 2]$ and $\phi_Y = [-\pi, +\pi]$ to obtain an

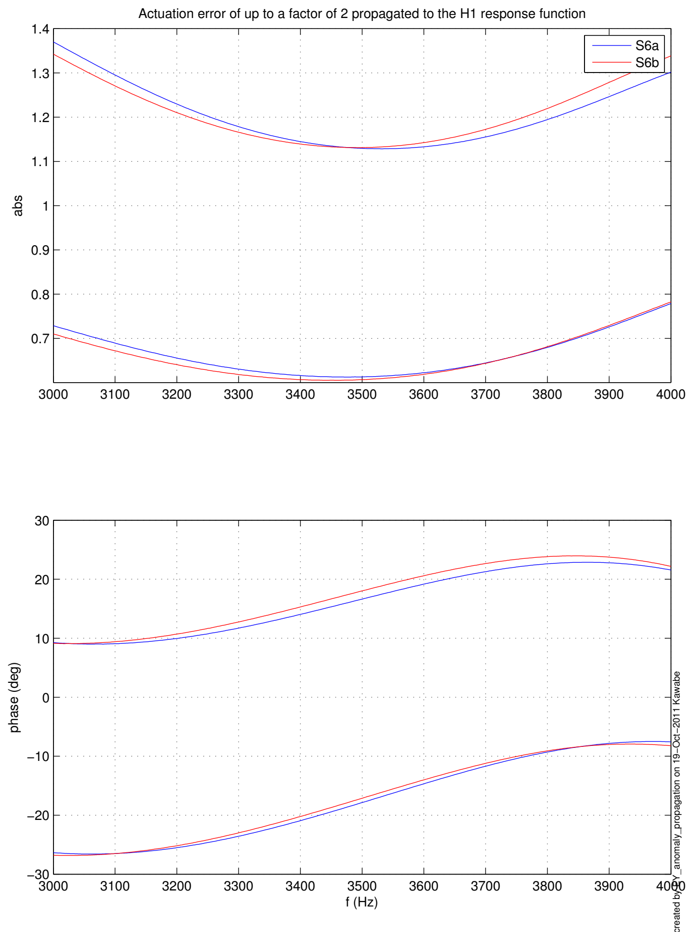

Figure 6.1: Upper and lower bound of the H1 response function error between 3000 and 4000 Hz assuming that θ_Y for H1 is within [0.5,2] range in amplitude and an arbitrary phase error, even at the true resonance peaks and valleys.

array of potential errors. Figure 6.1 shows the upper and lower bound of the error. From this plot, we obtain an inflated error of 40% in amplitude and 26 degrees in phase.

7 Timing Calibration

Throughout the entire science run, three numbers related to the timing of the sensing have been measured and tracked. These are the ADC timing error (τ_{ADC}), the OMC-LSC latency error (τ_{CPU}), and the time part of the whitening/dewhitening mismatch (τ_{wh}). The timing error of the calibrated data of LIGO instruments is represented by the sum of these and an

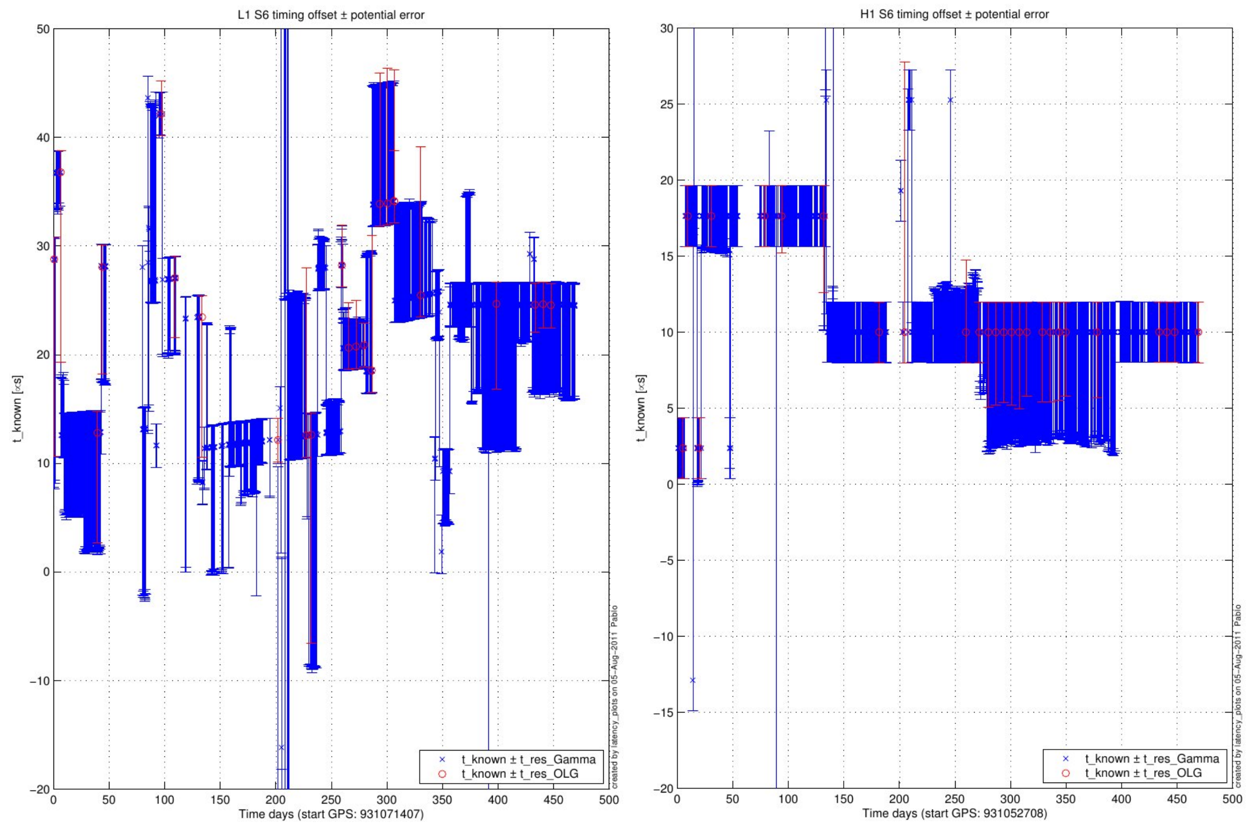

Figure 7.1: Timing error of L1 (left) and H1 (right) for the entire S6. The timing error itself is derived from the known systematic in the sensing, but the error bar is set by two different techniques. Blue and red traces represent the error bars obtained from the coil calibration line and the OLG. Though the OLG data provides more accurate measure of the true timing than the calibration line data, tha latter is calculated for all science segments.

error bar:

$$\tau_{V2} = \tau_{ADC} + \tau_{CPU} + \tau_{wh} + \delta\tau^{+}_{V2} - \delta\tau^{-}_{V2}. \tag{7.1}$$

Sign convention is such that a positive number means the true sensing function is delayed from the V2 model, i.e. the calibrated V2 data should be advanced to match the physical strain.

We have four sets of measurements that can be used for verifying the above timing and for defining the error bar, i.e. the latency mismatch measured by the OLG, the phase mismatch constantly monitored by the coil calibration line at around 1.1 kHz, the phase mismatch constantly monitored by the photon calibrator at around 400 Hz and the phase mismatch measured by the photon calibrator at around 100 Hz.

The latency mismatch measured by the OLG (4.1.9), τ_G, doesn't include any phase systematics that is not proportional to the frequency, because the OLG is measured at many frequency points between 40 and 5000 Hz, against which a linear phase fit is applied to get τ_G. The latency residual of an unknown origin is defined by

$$\tau_G^{unknown} = \tau_G + \tau_{ADC} + \tau_{CPU} + \tau_{wh} - \tau_M \tag{7.2}$$

where τ_M is the actuation delay of unknown origin in the model. Take extra care of the sign convention here: Positive τ_G means a smaller delay (or a time advancement) in the actual servo than the model, ditto for τ_M, while positive τ_{ADC}, τ_{CPU} and τ_{wh} means a larger delay. This latency residual is closely related to the timing error bar. If this is in the sensing, the LIGO timing is systematically off by the same amount. Even though it most likely originates in the timing systematic in the actuation, we cannot prove it as the S/N of the actuation timing monitor circuit was not good enough to draw any meaningful data.

Though the OLG latency mismatch gives the true measure of latency, only a limited set of OLG measurements is available (24 measurements for L1 and 26 for H1 over the entire S6). However, we have been continuously monitoring the calibration line at about 1.1 kHz, and we can use this data in a similar manner as the OLG. Even though a single frequency measurement means that it includes both the latency mismatch as well as the phase systematic that is not proportional to the frequency, we can still use it as a conservative measure of the latency error. We have measured the calibration line for a few minutes per all version 4 science segments, and obtained the following unknown residual per each segment

$$\tau_{coil}^{unknown} = \tau_{coil} + \tau_{ADC} + \tau_{CPU} + \tau_{wh} - \tau_M \tag{7.3}$$

where τ_{coil} is the equivalent latency mismatch obtained from the measurement at the calibration line frequency.

Since $\tau_G^{unknown}$ was about 2 μs in late S6 where we checked the actuation timing in both L1 and H1, we claim that our error in the timing cannot be smaller than 2 μs. As a conservative measure, we took the largert and smallest number possible for the timing error bar as follows:

$$\delta\tau_{V2}^{+} = \max(2\mu\text{s}, \tau_{G}^{unknown}) \text{ or } \max(2\mu\text{s}, \tau_{coil}^{unknown}) \quad (7.4)$$

$$\delta\tau_{V2}^{-} = \min(-2\mu\text{s}, \tau_{G}^{unknown}) \text{ or } \min(-2\mu\text{s}, \tau_{coil}^{unknown}). \quad (7.5)$$

Figure 7.1 shows the timing error represented by Equations 7.1, 7.4 and 7.5. Based on this analysis, a timing error was determined to be $[-10, 45]$ μs for L1 and $[0, 30]$ μs for H1. A calibration data flag is going to be made [3,4] using the following criteria:

- Timing error threshold is $[-10, 45]$ μs for L1 and $[0, 30]$ μs for H1.
- Any science segment is flagged if τ_{V2} is out of the above threshold.
- Even if τ_{V2} doesn't exceed the threshold, the science segment is still flagged if the error bar width $\delta\tau_{V2}^{+} - \delta\tau_{V2}^{-}$ is larger than the width of the threshold.

There are two phase systematic measurements using the photon calibrator. One was done by monitoring the lines constantly injected by the photon calibrator at around 400 Hz, the data of which was available for the entire S6 [5,6]. The other used two lines at about 110 Hz separated by 1 Hz that was temporarily injected out of the science time [7]. Being basically single frequency measurements, just like coil calibration line measurement at 1.1 kHz these cannot separate the timing from other phase systematics, but they are extremely useful as the photon calibrator was the only method in S6 that measured the response of LIGO instruments independently of the coil actuators. Both of these measurements agreed well with the timing and phase error budget of S6.

For example, two of the 110 Hz measurements for L1 claimed about 100 μs or 4 degrees of delay in the calibrated $h(t)$ data in July and October 2010, or 376 and 459 days from the start of S6. On the other hand, at the time of these measurements, the L1 timing delay was about 24 μs with the errorbar smaller than 10 μs according to Figure 7.1, which is equivalent of 1 degree with an error bar smaller than 0.5 degrees at 100 Hz. Both of the measurements

Error	Origin	L1	H1
Frequency dependence of the actuation electronics	A	<2%, 0.6 degrees	<1.5%, 0.7 degrees
Optical spring	A and C	<1% at 40Hz, becomes smaller by $1/f^2$	
Drumhead notch	A and C	<0.1%, 0.1 degrees	<0.12%, 0.7 degrees
Violin2 notch for L1	A	<1% 0.5 degrees except [600 800] Hz	none

Table 9: Errors not explicitly put in the error budget. Violin notch refers to an out-of-configuration operation of L1 that affected a small number of science segments that were flagged. Note that the combined effect of all of these except Violing2 should be consistent with the unknown part of OLG residual plus the error in the OLG.

were done when the L1 configuration corresponded to the third S6b configuration in the error budget plot (Figure 4.17 right, magenta traces), which gives about 3.5 ± 1.5 degrees of phase delay at 110Hz. Note that the sign convention in the error budget plot is that the positive phase means that the LIGO calibrated data is delayed. Therefore LIGO error budget gives $3.5 + 1 \pm 1.5 = 4.5 \pm 1.5$ degrees. The agreement with the photon calibrator measurement is very good.

8 Systematics Not Explicitly Put in the Error Budget

All known systematics that were not explicitly put into the error budget analysis are discussed here. Table 9 shows the errors and their magnitude. The fact that these were not put into the error budget does not mean that the effect of these are ignored. Quite contrary, the combined effect of these are indirectly put into the error budget analysis via unknown part of OLG residual and the OLG error. There is only one systematic that is not entirely negligible (frequency dependence of the actuation electronics), and we'll see if this is consistent with the unknown part of the OLG residual.

8.1 Actuation Electronics Frequency Dependence

Frequency dependence of the actuation electronics was measured using a coil current monitor, and is shown in Fig.8.1. Though this is not explicitly put into the error budget, this is

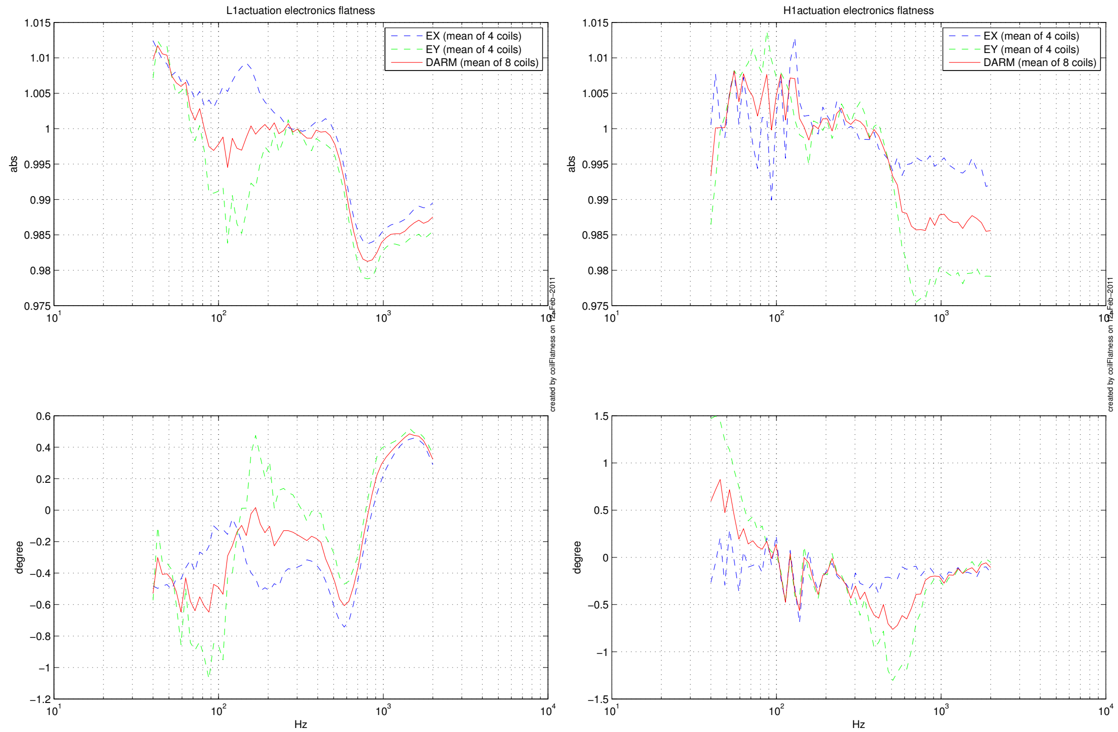

Figure 8.1: Actuation electronics frequency dependence.

consistent with the unknown OLG mismatch (see Fig.4.14). We can safely say that this is correctly taken care of by $Res_M^U \theta_{OLG}$.

8.2 Optical Spring Due To Radiation Pressure

Radiation pressure exerted on the test masses by the light circulating in the arm cavities is the function of the length of the arms. Depending on the deviation from the exact resonance, the radiation pressure can work like a normal spring (when the length is longer than the exact resonance) or a negative spring (shorter). In eLIGO interferometers, since both of the arms have offset from the resonance point, but with opposite signs, one arm has positive optical spring making the pendular resonance "stiffer", and the other arm becomes "softer" (or unstable depending on the amplitude of the optical spring) with negative spring.

This only affects the calibration of the actuation chain at lower frequency. For eLIGO calibration band of [40, 5000] Hz, both a first-principle calculation and a comparison of open loop transfer function measurements at two different laser power levels show that this is

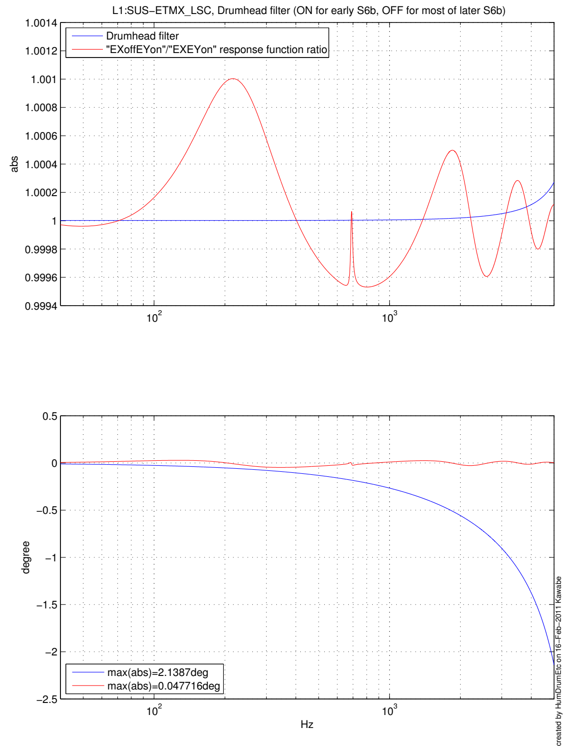

Figure 8.2: Drumhead notch effect for L1, which is very small and is safely ignored in the error analysis. Blue trace shows the filter itself, while red shows the DARM response function ratio of “EX notch off” over “both on”.

negligible[8].

8.3 Drumhead notch

For S6b, a new OMC alignment method was developed that necessitates to turn off all notch filters for ETMX that suppresses the drumhead mode at 9kHz. For L1, this only means that one notch filter in ETMX (named “Drumhead”) is turned off, while for H1 both ETMX (“TMnotch”) and OMC (“HumDrum9k”) notch filters are turned off.

Whether or not to use this new alignment method was left for the operators/SciMons depending on the behavior of the IFOs, and therefore both of the configurations (“Drumhead ON” and “Drumhead OFF” for L1, “TMnotch and HumDrum9k ON” and “TMnotch and HumDrum9k OFF”) are considered normal.

As shown in Figs.8.2 and 8.3, the difference between “drumhead on” and “off” is so small that these configurations can be practically considered identical.

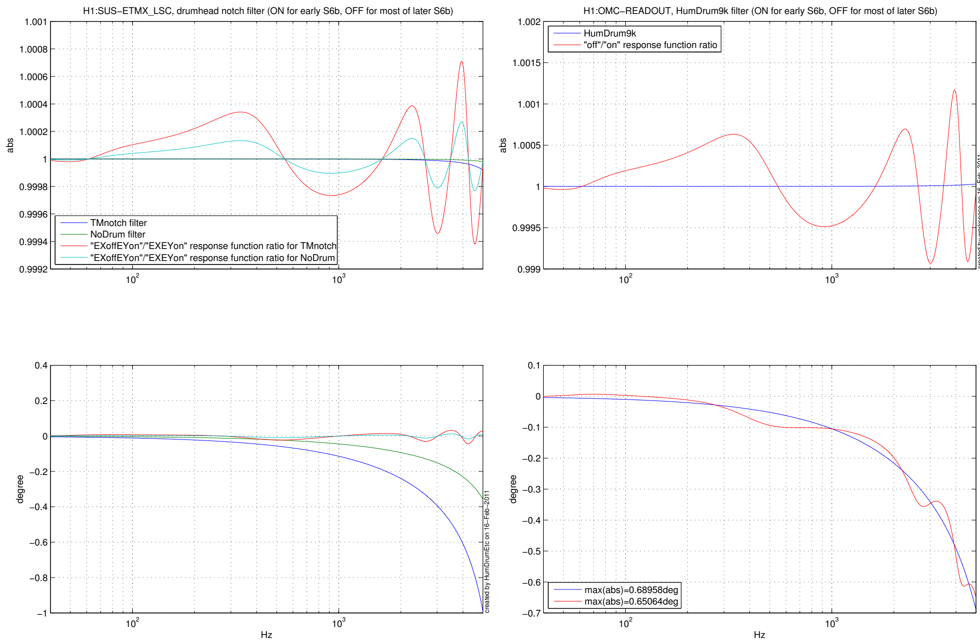

Figure 8.3: Drumhead notch effect for H1. This is safely ignored in the error analysis.

8.4 Violin2 Notch for L1 ETMX

The notch filter for the second violin mode resonance for L1 ETMX, which is supposed to be always on, was turned off for relatively small number of science segments within a period of about two weeks between Mar/24/2010 and Apr/8/2010. The segments affected were flagged as L1:DCH-ETMX_VIOLIN2OFF:1.

The calibration is not affected except a narrow band between 600 and 800 Hz as shown by the red trace in 8.4. Analysis groups should judge by themselves if their analyses are vulnerable to this.

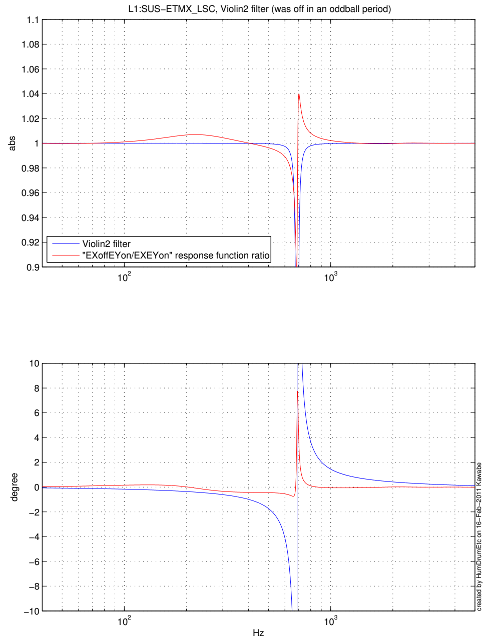

Figure 8.4: L1 EX violin2 filter effect. Red trace shows how the response function is altered when this filter is mistakenly disabled. Only a small number of segments were found to be with this configuration, and were flagged as L1:DCH-ETMX_VIOLIN2OFF:1.

9 Appendix

9.1 Propagation of OLG Error to CLG Error

Suppose that we have a measurement of an arbitrary transfer function G with an amplitude error bar and the phase error bar:

$$|G| = G_0 \pm \delta a \tag{9.1}$$

$$\delta a \equiv \mathrm{std}(|G|) \tag{9.2}$$

$$\angle G = \psi_0 \pm \delta\psi \tag{9.3}$$

$$\delta\psi \equiv \mathrm{std}(\angle G) \tag{9.4}$$

where G_0 and ψ_0 are the mean amplitude and the phase, while δa and $\delta\psi$ are the standard deviation of the amplitude and the phase. We want to propagate δa and $\delta\psi$ to the error of $CLG = 1 + G$. Figure 9.1 left shows CLG and G in a measurement coordinate system where

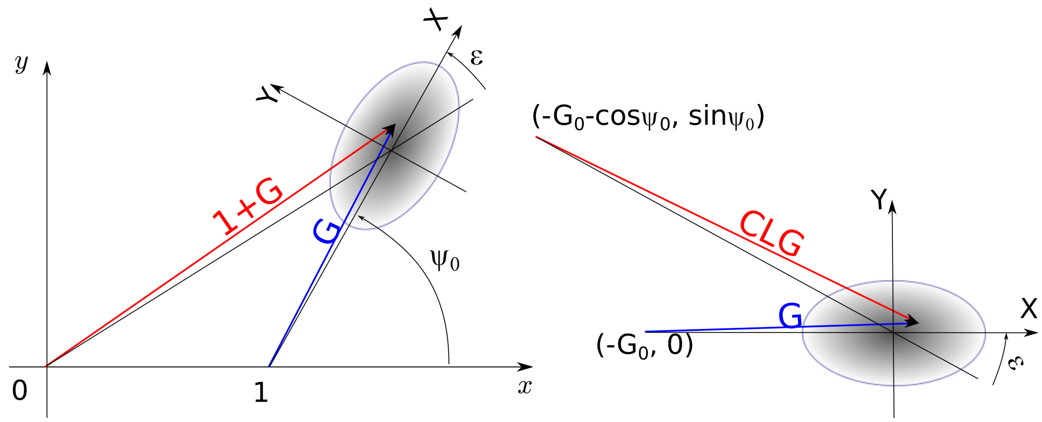

Figure 9.1: Open loop transfer function G (blue) and closed loop transfer function $1 + G$ (red). The elliptical blob shows the error distribution. The mean of $1 + G$ is centered at the origin of a new coordinate (X, Y) (right).

x and y are the real and imaginary part, respectively.

The calculation becomes simpler when you move to a coordinate system (X, Y) in which the error blob is centered at the origin and the mean of G is a real number (Figure 9.1 left).

$$
\begin{aligned}
G &= G_0 + X + iY && (9.5)\\
\mathrm{std}(X) &= \delta a && (9.6)\\
\angle G &= \mathrm{atan}\left(\frac{Y}{G_0 + X}\right) && (9.7)\\
\mathrm{std}(\angle G) &= \delta\psi \\
&\sim \mathrm{std}\left(\frac{Y}{G_0 + X}\right) \\
&\sim \mathrm{std}(Y)/G_0. && (9.8)
\end{aligned}
$$

CLG is written by

$$
\begin{aligned}
CLG &= G_0 + X + \cos\psi_0 + i(Y - \sin\psi_0) && (9.9)\\
|CLG| &\sim \sqrt{G_0^2 + 2G_0\cos\psi_0 + 1}\left[1 + \frac{X(G_0+\cos\psi_0) - Y\sin\psi_0}{G_0^2 + 2G_0\cos\psi_0 + 1}\right] \\
&= |<CLG>| + X\cos\epsilon - Y\sin\epsilon && (9.10)\\
|<CLG>| &= \sqrt{G_0^2 + 2G_0\cos\psi_0 + 1} && (9.11)\\
\tan\epsilon &\equiv \frac{\sin\psi_0}{G_0 + \cos\psi_0} && (9.12)\\
\angle CLG &= \mathrm{atan}\frac{Y - \sin\psi_0}{G_0 + \cos\psi_0 + X} \\
&\sim \mathrm{atan}\left[-(1 - \frac{X}{G_0+\cos\psi_0} - \frac{Y}{\sin\psi_0}) \times \frac{\sin\psi_0}{G_0+\cos\psi_0}\right] \\
&= -\mathrm{atan}\left[(1 - \frac{X}{|<CLG>|\cos\epsilon} - \frac{Y}{|<CLG>|\sin\epsilon})\tan\epsilon\right] \\
&\sim -\epsilon - \cos\epsilon\sin\epsilon\left[-\frac{X}{|<CLG>|\cos\epsilon} - \frac{Y}{|<CLG>|\sin\epsilon}\right] \\
&= -\epsilon + \frac{1}{|<CLG>|}(X\sin\epsilon + Y\cos\epsilon). && (9.13)
\end{aligned}
$$

Using Eqs. 9.1-9.13, the standard deviation of the amplitude and phase of CLG is written by

$$
\begin{aligned}
\mathrm{std}(|CLG|) &= \sqrt{(\delta a\cos\epsilon)^2 + (G_0\delta\psi\sin\epsilon)^2} \\
&= \sqrt{\mathrm{std}^2(|G|)\cos^2\epsilon + <|G|>^2\,\mathrm{std}^2(\angle G)\sin^2\epsilon} && (9.14)\\
\mathrm{std}(\angle CLG) &= \frac{\sqrt{\mathrm{std}^2(|G|)\sin^2\epsilon + <|G|>^2\,\mathrm{std}^2(\angle G)\cos^2\epsilon}}{|<CLG>|}. && (9.15)
\end{aligned}
$$

If G is written by

$$
G = G_M|\theta_{OLG}|\exp i(2\pi f\tau_G + \Delta\phi_{OLG}), \qquad (9.16)
$$

we can put the following into Eqs.9.14 and 9.15

$$
\begin{aligned}
<|G|> &= |G_M| < |\theta_{OLG}| > \quad (9.17)\\
\mathrm{std}(|G|) &= |G_M| \mathrm{std}(|\theta_{OLG}|) \quad (9.18)\\
\mathrm{std}(\angle G) &= \mathrm{std}(\Delta\phi_{OLG}) \quad (9.19)
\end{aligned}
$$

(note that G_M and τ_G are not statistical variables) to obtain the closed loop gain errors in Eqs.4.24 and 4.25:

$$
\begin{aligned}
\mathrm{std}(|\eta_{1+G}|) &= \mathrm{std}\left(\frac{|1+G|}{|1+G_M|}\right)\\
&= \frac{|G_M|\sqrt{\mathrm{std}^2(|\theta_{OLG}|)\cos^2\epsilon + <|\theta_{OLG}|>^2 \mathrm{std}^2(\Delta\phi_{OLG})\sin^2\epsilon}}{|1+G_M|} \quad (9.20)\\
\mathrm{std}\left(\angle\frac{1+G}{1+G_M}\right) &= \mathrm{std}\left(\angle(1+G)\right) \quad (9.21)\\
&= \frac{|G_M|\sqrt{\mathrm{std}^2(|\theta_{OLG}|)\sin^2\epsilon + <|\theta_{OLG}|>^2 \mathrm{std}^2(\Delta\phi_{OLG})\cos^2\epsilon}}{|<1+G_M|\theta_{OLG}|\exp i(2\pi f\tau_G + \Delta\phi_{OLG})>|} \quad (9.22)\\
&\sim \frac{|G_M|\sqrt{\mathrm{std}^2(|\theta_{OLG}|)\sin^2\epsilon + <|\theta_{OLG}|>^2 \mathrm{std}^2(\Delta\phi_{OLG})\cos^2\epsilon}}{|1+G_M<|\theta_{OLG}|>\exp i(2\pi f\tau_G + <\Delta\phi_{OLG}>)|} \quad (9.23)
\end{aligned}
$$

9.2 Adding CLG Error and Sensing Error Coherently

As was described in 4.4, there is a case where we need to assume that the error bar in the sensing and the closed loop response are 100% positively correlated. An

error bar of a quantity defined by $(1+G)/G = 1 + 1/G$ needs to be calculated. Using the same notation as 9.5-9.8, absolute value and phase of $1/G$ are represented by

$$
\begin{aligned}
\left\langle\left|\frac{1}{G}\right|\right\rangle &= \frac{1}{G_0} \quad (9.24)\\
\mathrm{std}\left(\left|\frac{1}{G}\right|\right) &= \frac{\mathrm{std}(|G|)}{G_0^2} \quad (9.25)\\
\left\langle\angle\frac{1}{G}\right\rangle &= -\psi_0 \quad (9.26)\\
\mathrm{std}\left(\angle\frac{1}{G}\right) &= \mathrm{std}\left(\angle G\right). \quad (9.27)
\end{aligned}
$$

Substituting all quantities related to G with the ones related to $1/G$ in Eqs.9.14 and 9.15, and using Eqs.9.24-9.27, we obtain the following:

$$\tan\kappa \equiv \frac{-\sin\psi_0}{1/G_0 + \cos\psi_0} \tag{9.28}$$

$$\begin{aligned} \mathrm{std}\left(\left|1+\frac{1}{G}\right|\right) &= \sqrt{\mathrm{std}^2\left(\left|\frac{1}{G}\right|\right)\cos^2\kappa + \left\langle\left|\frac{1}{G}\right|\right\rangle^2 \mathrm{std}^2\left(\angle\frac{1}{G}\right)\sin^2\kappa} \\ &= \frac{\sqrt{\mathrm{std}^2\left(|G|\right)\cos^2\kappa + G_0^2\mathrm{std}^2\left(\angle G\right)\sin^2\kappa}}{G_0^2} \end{aligned} \tag{9.29}$$

$$\mathrm{std}\left(\angle(1+\frac{1}{G})\right) = \frac{\sqrt{\mathrm{std}^2\left(|G|\right)\sin^2\kappa + G_0^2\mathrm{std}^2\left(\angle G\right)\cos^2\kappa}}{G_0^2\,|< 1 + 1/G >|}. \tag{9.30}$$

9.3 List of Configurations in S6

In S6, due to various reasons we have multiple configurations for the sensing hardware and/or software in a single calibration epoch. Table 10 shows the gps time each of these configurations was used.

9.4 Blind Injection

At GPS time 968654558, a hardware injection was performed on L1, H1 and Virgo instrument at the same time without the knowledge of the LIGO and Virgo personels except a few. This "blind" injection event was handled as a real astronomical event candidate until the blind injection committee revealed the nature of the event.

Using the systematics obtained from the hardware configurations and the latency mismatch of -13.3μs for L1 and -1.6μs for H1 that were measured both before and after the event, it's possible to do a finer grained analysis for the calibration of this event. Figure 9.2 shows the frequency dependent part of the error for both L1 and H1. There are two things to note.

First, the error bar of the calibration systematic is very small compared to the entire run. Note that the code discards some errors (most notably the statistical measurement error for the estimate of Gamma systematic that is up to about 1%) and therefore the actual error

S6a	S6b	IFO
L1 S6a wh/dw 1: [931071407, 931219000]	L1 S6b wh/dw 1 (*): [939020344, 957229000] [957247016, 957567100]	L1
L1 S6a wh/dw 2 (*): [931219808, 937984100]	L1 S6b wh/dw 2: [957229340, 957246400]	
L1 S6a wh/dw 3: [937984783, 938316000] [938370827, end of S6a]	L1 S6b wh/dw 3 (I): [957567771, 968092000] [968261889, 968411200] [968436964, end of S6b]	
L1 S6a wh/dw 4: [938316290, 938370200]	L1 S6b wh/dw 4: [968092571, 968261300]	
	L1 S6b wh/dw 5: [968411871, 968436300]	
H1 S6a wh/dw 1: [931052708, end of S6a]	H1 S6b wh/dw 1: [948444884, 948539900]	H1
	H1 S6b wh/dw 2: [961827382, 961835000]	
	H1 S6b wh/dw 3 (*)(I): [942440116, 948444200] [948540482, 961826800] [961835601, end of S6b]	

Table 10: Table of gps time per each configuration. Nominally correct configuration and blind injection are indicated as (*) and (I). Two GPS time in a bracket means that any science segments in this specific range belongs to the configuration shown in the left column. Sometimes there are more than one ranges for one configuration.

bar is as large as 1 or 2 %, but this is already very good.

Second, the systematic error is significantly larger in L1 than in H1, and L1 error budget is not compatible with what was originally reported to the LVC detection committee. One of the two reasons for this is that the S6b whitening/dewhitening configuration information, which was originally obtained by manually searching through the filter archive, was incorrect, which made us underestimate the systematic by up to 4% depending on the frequency. This was fixed after we implemented a script to automatically search for any changes in the filter archive. A greater impact, though, came from the fact that the effect of Gamma systematic (as opposed to the Gamma error due to the measurement noise) was not originally taken into account. Because L1 was not in the nominally correct S6b configuration, our estimate of Gamma factor was about 4% larger systematically than it should be, and this is amplified

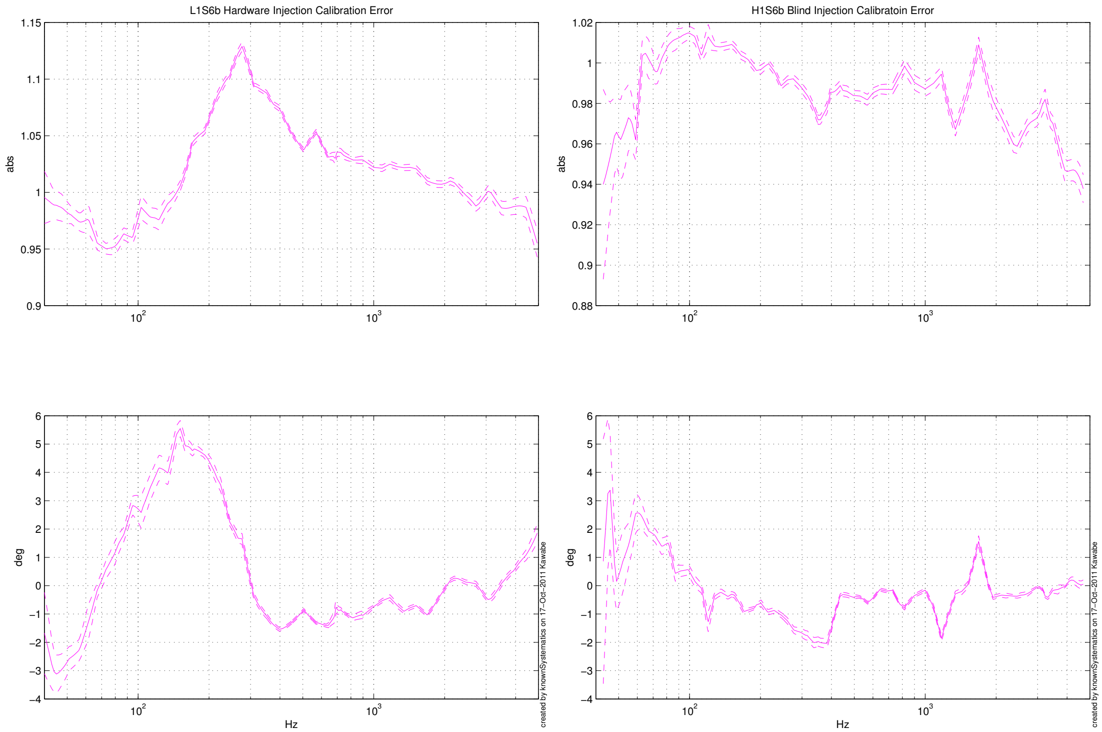

Figure 9.2: Calibration error of LIGO instruments at GPS time 968654558.

by up to about a factor of 2 (i.e. 8 to 9 %) due to the closed loop response of the control loop between 200 and 400 Hz. The overall error of L1 was dominated by the 15% scaling error bar originally, but now we know that the frequency dependent systematic of about 12% at around 270 Hz is comparable to the scaling error bar. Impact of Gamma factor systematic on H1 is not as large as L1, since H1 was running in a nominally correct S6b configuration.

In addition, a closer look at the timing plot (Figure 7.1) shows that L1 and H1 response function was 24.5 μs and 10.0 μs delayed relative to the physical strain for this event, with about 2 μs uncertainty.

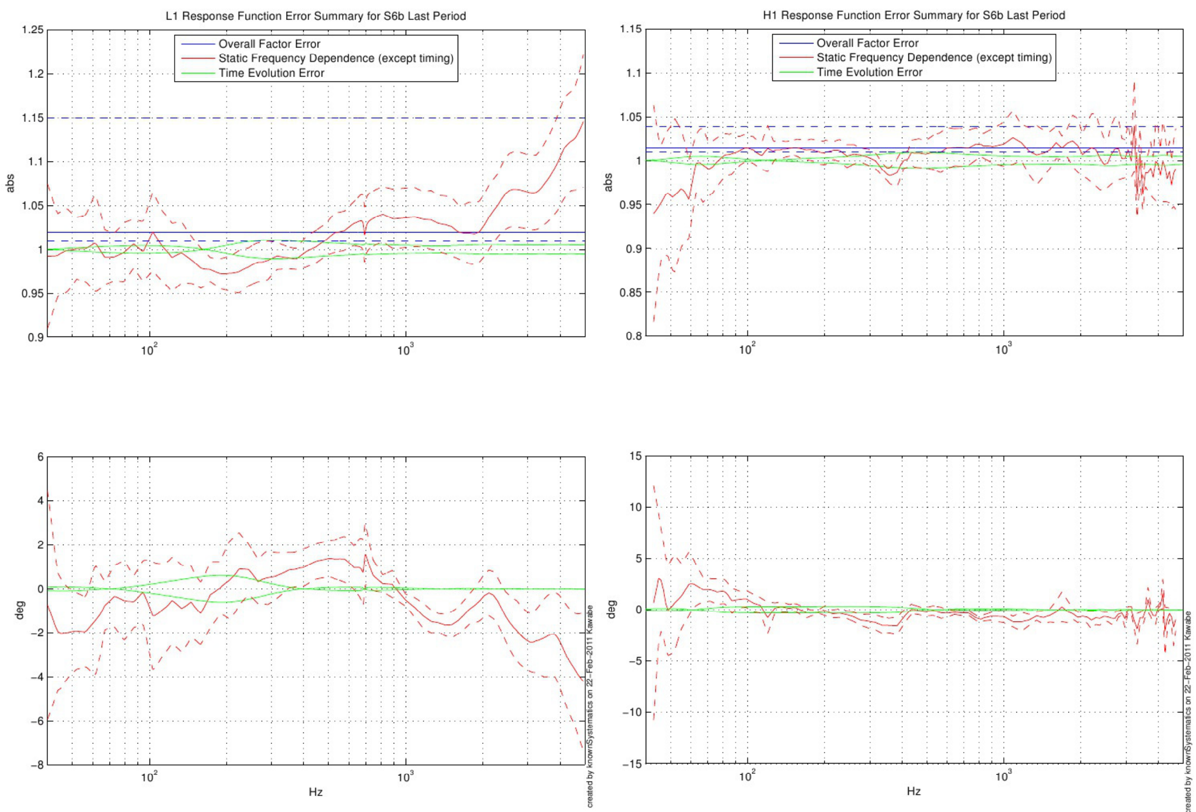

Figure 9.3: Blind injection calibration that was originally reported to the LVC detection committee. L1 data is not compatible with the latest error estimate for GPS time of 968654558 (Figure 9.2) any more.

IFO	V2 OLG latency error	V2 ad-hoc delay	ADC delay	OMC-LSC latency error	Whitening delay	Residual
L1	τ_G =-13.3 μs	τ_M =9.0 μs	τ_{ADC} =17.3 μs	$\tau_{CPU} = 0$	τ_{wh} =7.2 μs	+2.2 μs
H1	τ_G =-1.6 μs	τ_M =10.1 μs	τ_{ADC} =1.2 μs	$\tau_{CPU} = 0$	τ_{wh} =8.8 μs	-1.7 μs

Table 11: Timing budget using the last three (L1) or four (H1) measurements of OLG corresponding to the last part of the second calibration epoch starting 14/Sep/2010. Residual represents the truly unknown systematic, and is obtained by $\tau_G - \tau_M + \tau_{ADC} + \tau_{CPU} + \tau_{wh}$. The sensing delay that is not accounted for in the V2 model is equal to the delay of the calibrated frequency domain strain signal, and is represented by $\tau_{ADC} + \tau_{CPU} + \tau_{wh}$ (24.5 μs for L1 and 10.0 μs for H1, a positive number means the response function has an additional delay).

References

1. http://blue.ligo-wa.caltech.edu:8000/mLIGO/S6Calibration/Review/HighFreq

2. http://lhocds.ligo-wa.caltech.edu:8000/mLIGO/S6Calibration/Review/Actuation

3. L1 bad timing flagged segments: https://svn.ligo.caltech.edu/svn/calibration/trunk/calibration/frequ

4. H1 bad timing segments: https://svn.ligo.caltech.edu/svn/calibration/trunk/calibration/frequencyd

5. J. Berliner, H. P. Daveloza, R. Savage, "Timing of L1 in S6 via the Photon Calibrator" LIGO-T1000721

6. J. Berliner, H. P. Daveloza, R. Savage, "Timing of H1 in S6 via the Photon Calibrator", LIGO-T1000743

7. I. Bartos et. al, "Timing Performance Verification Studies - S6 Photon Calibrator Results", LIGO-T1000638

8. http://lhocds.ligo-wa.caltech.edu:8000/mLIGO/S6Calibration/Review/Actuation#OpticalSpring